Towards Video-Based Power Estimation in Speed Skating

Determining Mechanical Power and Push-Off Force in Long-Track Speed Skating Using Only Kinematic Data.

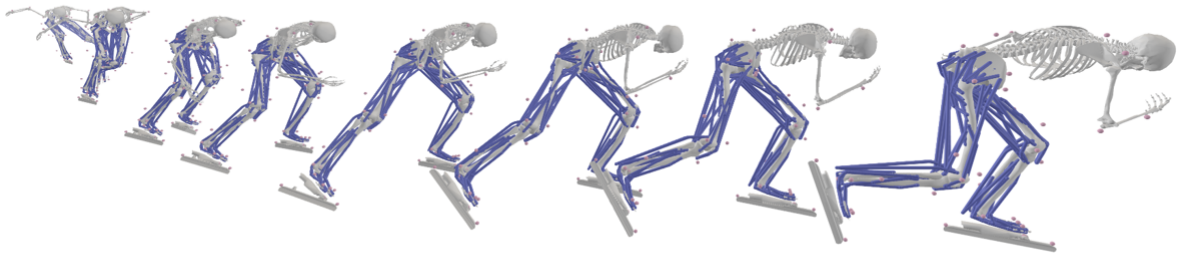

Msc. Thesis Biomedical Engineering

Author	Ragnhild Maarleveld
Supervisor	Eline van der Kruk

October 26, 2024

Contents

1 Abstract

Mechanical power combined with the forward velocity of the skater on the ice rink is a useful indication of the efficiency of the technique. This can be determined by measuring the push-off forces and angular joint velocities of the ankle, knee, and hip. These measurements often require extensive set-up time and equipment.

Recent advancements in single-camera, markerless estimation of 3D kinematics are promising. Additionally, prior research established a verified "Simple Skater Model" that accurately replicates observed push-off forces using only kinematic input.

Therefore, we developed a Matlab pipeline to assess mechanical power in long-track speed skating using only kinematic data. This video-to-power approach was validated with kinematics from a motion capture system (Qualisys 2015) and forces measured with an instrumented klapskate.

We found a significant difference between the modeled and measured peak power ($p < 0.05$) and an interquartile range (IQR) of error percentages between 10.7% and 24.5% for all participants. For three of the four participants, the median errors were consistent at 18.9%, 23.1%, and 18.0%

Despite this margin, the peak power error is an acceptable compromise. The goal is to leverage mechanical power and skater velocity to gauge technique efficiency and track its progress over time in training or competition, especially when modifying training or technique. The primary objective of obtaining a readily quantifiable, kinematic-based power estimate was met, advancing video-to-power analysis developments.

2 Introduction

Speed skating is a competitive sport where athletes race against each other on the ice, striving for the fastest time over various distances, testing both speed and endurance. The Dutch have dominated speed skating internationally, regularly topping medal tables at World Championships and the Winter Olympics, and iconic events like the "Elfstedentocht" and the phenomenon of "Schaatskoorts" showcase how deeply ingrained speed skating is in Dutch culture and reflect the nation's enduring passion for the sport.

Gaining forward speed on the ice requires a complex motion. The simple backward push of a skate, familiar from walking, is not viable due to the low friction coefficient of the ice surface. Instead, skaters create forward speed by steering their skates to push sideways, resulting in a sinus-wave-like transverse trajectory of the upper body. Skaters must strike a balance between steering their skates sideways and moving forward. In addition to steering their skates, skaters lean their skates while applying force to them. [1]. The best speed skaters are characterized by balance, efficient use of metabolic energy, and an efficient technique where the rate of energy transfer, i.e. mechanical power, improves performance in terms of forward speed.

Mechanical power is thought to be of great value to coaches, sports scientists, and athletes [1],[2]. Typically, power output and endurance depend on the mechanical power sustained over a given distance [2]. As power includes environmental factors such as air friction, it is an objective measure to assess the external load of a training or competition and the fitness and fatigue of the athlete, preventing overtraining and helping training periodization [2]. The utilization of power in this way is a common practice in the field of cycling [3]. In speed skating, mechanical power combined with forward velocity is a useful indication of the efficiency of the technique.[1].

It is possible to obtain mechanical power in speed skating by measuring the kinematics and the push-off forces, as shown in the literature [4], [5], [6], [1]. However, these measurements frequently necessitate a considerable investment of time, resources, and expertise when it comes to the placement of passive reflective markers on the skater, installing the motion capture camera systems setup, the replacement of the bridges of the skate with instrumented bridges etcetera. This can disrupt the athlete's routine, as skaters prefer to minimize preparation time and avoid discomfort or loss of confidence in their equipment. In addition, these power measurements are most valuable when repeated over time to identify trends [2], but due to the time and cost of the current setup, are not practical for daily use.

However, recent advancements in single-camera video-based markerless estimation of 3D kinematics are proving to be highly promising, as demonstrated by Bittner et al [7].

Furthermore, Lin et all [8] demonstrated the great potential of the integration of deep learning 3D human pose estimation techniques for predicting joint kinematics and body segment scales with an underlying OpenSim skeletal model, validating the biomechanical fidelity of this pipeline. This eliminates the need for using a complex motion capture system with multiple cameras and passive reflective markers on the skater. Moreover, previous research has established a verified "Simple Skater Model" that accurately replicates the observed push-off forces based on kinematic input alone[1], eliminating the need for installing instrumented bridges to skates.

Therefore, the aim of this research is to develop a Matlab-based [9] pipeline for assessing mechanical power in long-track speed skating based on solely kinematic data as input, essential in a future real-time video-to-power algorithm. This is achieved through a combination of an inverse dynamics approach and a musculoskeletal model (OpenSim), utilizing the kinematics derived from the motion capture system (Qualisys 2015) and force output by the Simple Skater Model, retrieved from previous research [1]. The aforementioned approach is validated through a comparison of the mechanical power values obtained with those derived from the same methodology, but utilizing measured forces instead.

In summary, the main contributions of this paper are:

- The introduction of a ready-made Matlab-based pipeline for assessing mechanical power in long-track speed skating based on solely kinematic data as input.
- The development of a musculoskeletal OpenSim model representing a skater, to be used in our pipeline, by combining a self-made klapskate model to an opensource musculoskeletal model.
- The incorporation of data from skaters into OpenSim for the first time.
- The presentation of a comparative analysis of the joint power following from our pipeline with a kinematic-only based input and a measured input.

3 Method

3.1 Mechanical Power Calculation

For determining the mechanical power(P_{mech}) of a speed skater, we lay our focus on the lower limbs. Therefore, the mechanical power is determined by directly summing the joint powers(P_{joint}) of the ankle, knee, and hip. This is shown by Equation 3.2 in which k represents the ankle-, knee-, and hip joint.

These joint powers are obtained by multiplying the respective joint moments (M) and angular joint velocities (ω) in all the degrees of freedom of the joints. For calculating the joint power in this manner, we assume that there is no translation within a joint and only consider the rotational degrees of freedom. This is shown by Equation 3.1, in which n represents the degrees of freedom. In the ankle joint we consider flexion/extension and inversion/eversion (n=2), in the knee joint we incorporate flexion/extension(n=1), and in the hip joint, we take into account flexion/extension, adduction/abduction, and rotation (n=3).

$$P_k^{joint} = \sum_{n=1}^{N} (M_n \cdot \omega_n) \tag{3.1}$$

$$P_{mech} = \sum_{k=1}^{N} P_k^{joint} \tag{3.2}$$

3.2 Musculoskeletal model

To obtain the joint moments and joint angular velocities, it would be beneficial to utilise an opensource musculoskeletal model[10] that includes the knee-, hip- and ankle joints. To determine the most suitable model from the available Opensim lower limb muscle models [11] for our athletes, a literature review was conducted [12] to assess the muscle properties and demographics each model represents. We found that none of the available models accurately represented an athlete, nor was there sufficient data to develop a tailored model. Therefore, we selected the full-body Rajagopal 2015 model, which best represents a younger demographic and includes the degrees of freedom in the ankle, knee, and hips as mentioned in section 3.1 Additionally, we modeled the klapskate using a bridge attached to the foot, and with a blade connected to the bridge by a hinge joint with one degree of freedom (Figure 3.2).

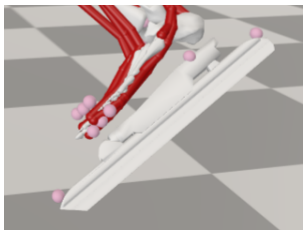

Figure 3.1: Skate body segment, skate closed

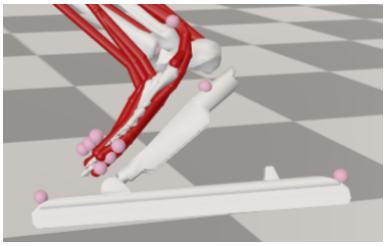

Figure 3.2: Skate body segment, skate open

3.3 Steps to Assess Mechanical Power

We propose a 7-steps kinematic-only methodology to assess the mechanical power. This is illustrated in the orange-colored boxes in Figure 3.3. The first step in this process is measuring the 3D kinematics. Subsequently, the musculoskeletal model is scaled to the participant (step 2) and follows the measured motion of the participant (inverse kinematics, step 3) to obtain the joint velocities. Then, the inputs for the simple skater model are obtained (step 4) and the forces are modelled (step 5). Thereafter, the OpenSim inverse dynamics tool is run to obtain the joint moments(step 6) and the mechanical power is obtained (step 7).

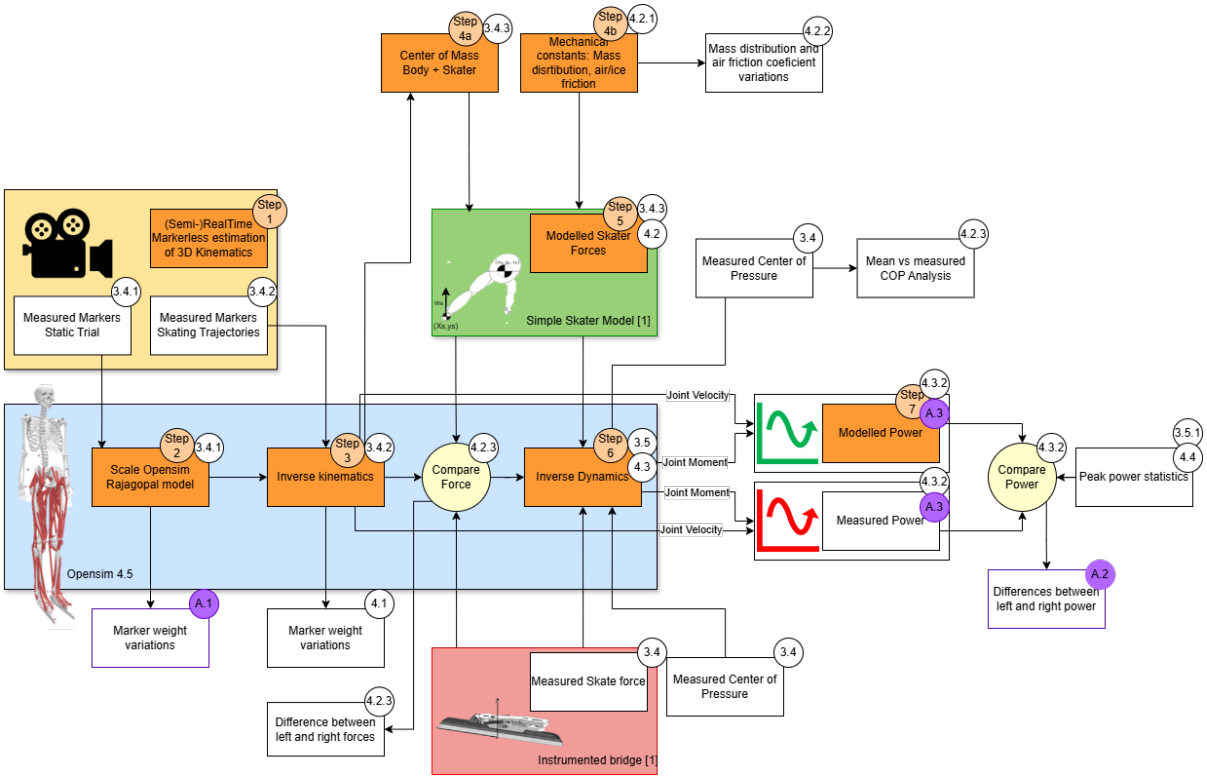

Figure 3.3: Overview of the steps for a kinematic-only methodology to assess the mechanical power output in long-track speed skating (orange coloured boxes) and the additional steps taken to validate this pipeline. Yellow box: Camera-based kinematics. Blue box: The OpenSim model and the Opensim Tools utilized. Green box: The Simple Skater Model. Red box: The instrumented bridge. Orange circles: represent the order of the kinematic-only methodology. White circles: The section in this report where the step is further explained. Purple circles: Appendix

3.4 Validation of the Steps to Assess Mechanical Power

To validate this seven-step approach, we perform the steps shown in Figure 3.3 utilising experimental data from a previous study [13]. This study collected three-dimensional long-track speed skating kinematics data and push-off forces from four professional speed skaters. The motion data was captured using a set of 20 motion capture cameras (300 Hz, Qualisys, 2015) over a distance of 50 metres along the straight section of the ice rink. The skater was equipped with 23 passive reflective markers attached to the suit (Figure 3.4) and skates (Figure 3.4) and wore instrumented bridges to measure the force and point of force application i.e. Center of Pressure (100Hz,interpolated to match to 300Hz marker recording). Multiple trial were recorded in which the participants were requested to skate at a constant velocity, selected by themselves, corresponding to the low (70%), medium (80%), and high (90%) intensity levels [1].

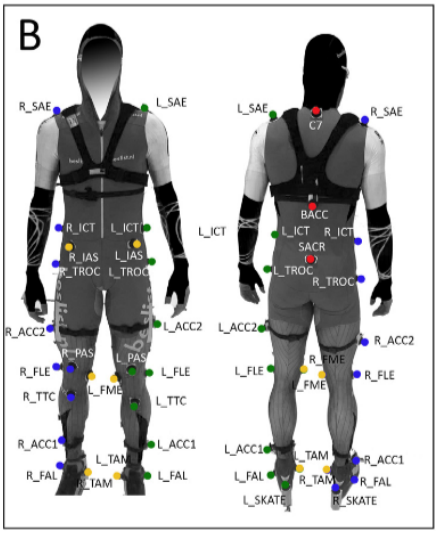

Figure 3.4: Body markers [1]. The yellow markers were removed for the dynamic trials

Figure 3.5: Skate markers [1]. The yellow markers were removed for the dynamic trials

3.4.1 Scaling

The recorded markers from a static trial were used to scale the Opensim model. To do this, we added the marker set used in the experiments (Figure 3.4,Figure 3.5) onto the model in OpenSim and compared this to the static pose measurement data (a recording of the participant standing upright for a few seconds).

The OpenSim "Scaling tool" goes through each time step (frame) of motion and computes generalized coordinate values which positions the model in a pose that "best matches" experimental marker and coordinate values for that time step. Mathematically, the "best match" is expressed as a weighted least squares problem, whose solution aims to minimize both marker and coordinate errors, as shown in Equation 3.3, where q is the vector of generalized coordinates being solved for, x_i^{exp} is the experimental position of marker i, xi(q) is the position of the corresponding model marker (which depends on the coordinate values), q_j^{exp} is the experimental value for coordinate j, w_i is the marker weight and w_j is the coordinate weight.

$$\min_{\mathbf{q}} \left[\sum_{i \in \text{ markers}} w_i \left\| \mathbf{x}_i^{\text{exp}} - \mathbf{x}_i(\mathbf{q}) \right\|^2 + \sum_{j \in \text{ unprescribed coords}} \omega_j \left(q_j^{\text{exp}} - q_j \right)^2 \right] \tag{3.3}$$

$$q_j = q_j \text{ for all prescribed coordinates } j \tag{3.4}$$

Directly scaling the model based on the distance between single markers is not advisable due to potential errors introduced by manual marker placement. Instead, we reduced this error by defining virtual markers based on a combination of multiple markers on bony landmarks (e.g. AJC, $Proj_{AJC}$, MFM25, KJC, HJC, MIAS, MHJC MPELV). The model's body segments were scaled according to the guidelines provided by OpenSim [14], illustrated in Figure 3.6-, Figure 3.8. We then defined static pose weight values, affecting to what degree a match should be satisfied. The magnitude of these weights is further explained in section A.1. It is important to note that the distances between the left leg

and right leg markers were averaged to ensure that both legs were the same size after scaling.

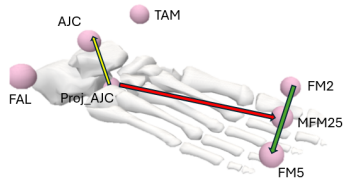

Figure 3.6: Foot scaling

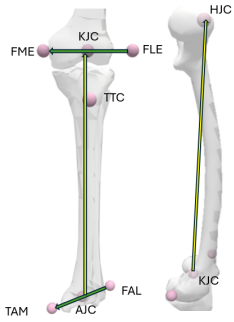

Figure 3.7: Femure and Tibia/Fibula scaling

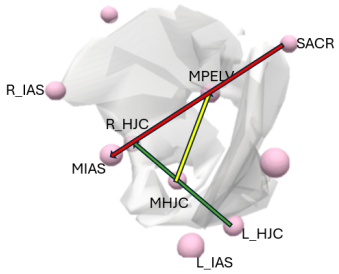

Figure 3.8: Pelvis scaling

3.4.2 Inverse Kinematics

The markers recorded when the participant was skating were used as an input for the OpenSim "Inverse Kinematics Tool" and the same least square problem Equation 3.3 was solved in every timestep (frame).

Markers on the blade were not recorded during these trials, causing the blade to follow the foot's movement (Figure 3.1) instead of remaining attached to the ice while exerting force (Figure 3.2). This misalignment affects the position of force application with respect to the joints, and therefore the calculated joint moments. To correct this, we reintroduced the "klapping motion" by describing the blade markers based on a vector from the hinge to the blade markers, and rotating this vector based on the force applied. When force was applied to the blade, the pitch angle was set to zero, describing a blade parallel to the ice. When there was no force applied to blade, the pitch angle of the blade followed the foot. The orientation of the foot during the trial was obtained using OpenSim's BodyKinematics analysis tool.

The Inverse Kinematics tool was initially operated with a marker weight of 1. However, it was anticipated that a few markers would display movement during the trial, potentially increase the associated marker error. This marker error could compromise the accurate representation of the participant's center of mass (B) and that of their skates (S) (see Figure 3.9), both of which are essential for calculating the push-off forces in the Simple Skater Model, as discussed in detail in subsection 3.4.3.

In particular, the markers in the shoulder area (SAE and C7), which were expected to move slightly backwards with the suit when the skater moved from the static pose into the skating position (bending forward), and the THIGH-(or ACC2 in Figure 3.4) and AnkleIMU marker (or ACC1 in Figure 3.4), as these were not attached to the suit but rather to a band around the thigh and ankle. Furthermore, it was possible that a few markers had been incorrectly recorded, which could result in high marker errors as well.

Therefore, a sensitivity analysis was subsequently conducted to assess the impact of varying the weights of the markers exhibiting a high marker error (i.e. around 10cm) and the SAE-, C7-, THIGH-, and AnkleIMU- markers, on the marker error and center of mass positions.

3.4.3 Forces

The next steps in the validation process included calculating the mechanical power (P_{Sim}) using the simple skater model forces (F_{Sim}) and calculating the mechanical power(F_{Meas}) using the actual measured forces (F_{Meas}).

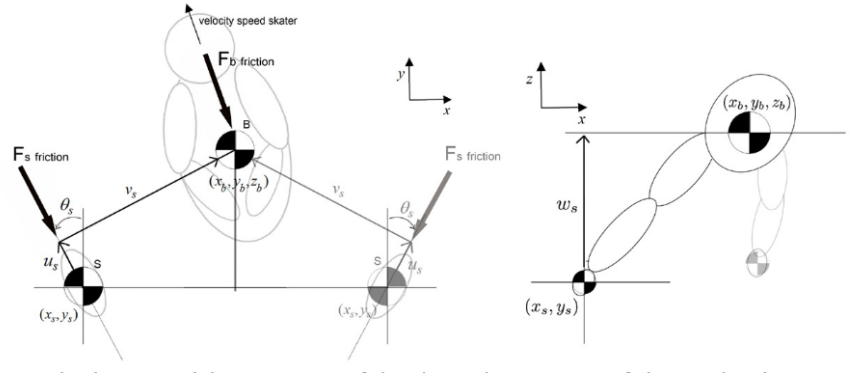

Figure 3.9: Simple Skater Model. Left: top view of the skater; Right: rear view of skater. B represents the CoM of the whole body, S represents the CoM of the skate.[1]

The simplified skater model considers the skater as a combination of three point masses: the body center of mass (B) and the left and right skate mass (S), as illustrated in Figure 3.9. Given the brief duration of the double stance phase, it was assumed that no double stance phase occurred. Therefore, only one skate is considered to be on the ice at a time, alternating between left and right. The alternation point is defined as the moment when forces exerted on both skates are equal. Consequently, only two masses are considered in the model at any given time, referred to as the active masses (mass B and one skate). The model's input includes the changing distance between the point mass position of the upper body and the skate (Euclidean distance in 3D space) (ie the leg extension) and skate steering angle. The output is the upper body motion of the skater in global space and the forces exerted by the skates on the ice. Errors in the upper body position, velocity, and force magnitude were accounted for, and the model's overall error (Jmin) was minimized by adjusting three mechanical constants: mass distribution, air friction, and ice friction coefficients.

An inspection of the sensitivity analysis of all the trials, which examines the impact of these mechanical constants on the model fit, reveals that the ice friction coefficient has the least effect (Figure 3.10. Consequently, it has been retained at 0.006 [1].

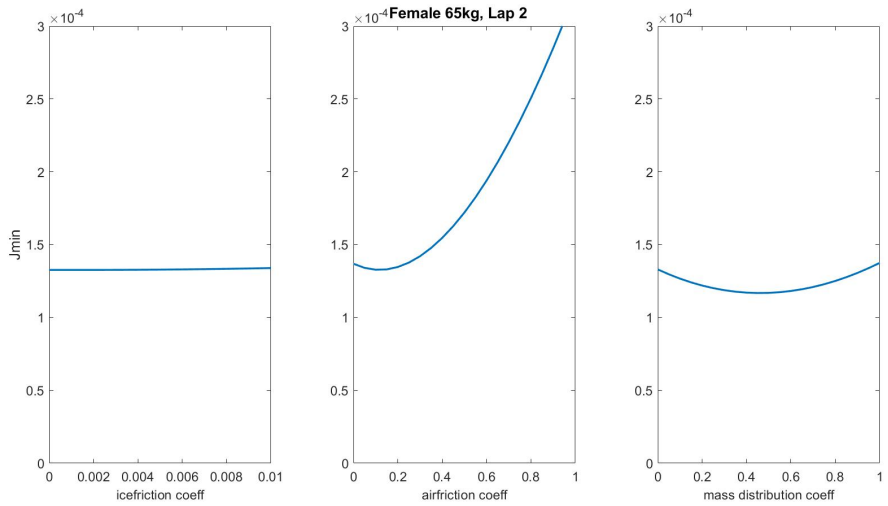

Figure 3.10: Example of a sensitivity analysis of the Female 65kg, Lap 2, showing the effect of changing the three mechanical constants: ice friction coefficient (mu), air friction coefficient (fric), mass distribution coefficient (alpha) on the Jmin error, representing the errors in the upper body position, upper body velocity, and the resultant force magnitude. The trends in airfriction and mass distribution results for Jmin differs between the trials, but the ice friction trends are similar.

Two approaches were considered for selecting the other two coefficients: using predetermined values from literature or optimizing them to minimize Jmin. Given the potential discrepancies in predetermined values in both mass distribution (Opensim model body masses vs real body masses) and air friction (values derived from the literature [15],[16] vs in real life), and the high sensitivity of the simplified model to air friction, we opted for optimization to derive the mechanical constants that yielded the smallest Jmin error. We keep in mind that the mass distribution can be on the high side due to the skater's lower leg having large muscles, but it is not likely to be higher than 0.6. Furthermore, based on the literature values for different skating configurations (High Trunk, Arm Loose etc) we expect a friction coefficient between 0.2 and 0.3 ($\frac{CdA}{0.5*\rho}$).

3.5 Inverse Dynamics

The subsequent step is to run the 'Ínverse Dynamics Tool' in OpenSim using the motion from the inverse dynamics step and the modelled forces to obtain the joint moments. In this step we also need the point of force application with respect to the blade (CoP). The simple skater model does not describe the point where force is applied to the blade. Therefore, in the validation process we used the measured CoP. For the kinematic-only methodology one should rather use the mean CoP of the measured trials. Therefore, we explored the impact of using the mean CoP of either all the right-, left-, or combined left and right skate strokes per participant, or of all participants combined, on the mechanical power output.

The Inverse Dynamics Tool solves the equations of motion as represented by Equation 3.5, where q, $\dot{q}$, $\ddot{q}$ are the position, velocity, and acceleration of the joint angles. M,

C, G are the mass, centrifugal and Coriolis, and gravitational forces matrices, respectively, whereas τ is the vector of unknown joint moments. Opensim likely solves these equations via a standard bottom-up approach [17], but no reference of this could be found.

$$\underbrace{\mathbf{M}(\mathbf{q})\ddot{\mathbf{q}} + \mathbf{C}(\mathbf{q}, \dot{\mathbf{q}}) + \mathbf{G}(\mathbf{q})}_{\text{knowns}} = \underbrace{\tau}_{\text{unknowns}} \tag{3.5}$$

3.5.1 Statistics

The final stage of the validation process for the proposed kinematics-only approach is a comparison of the two power outputs P_{Sim} and P_{Meas}. This is achieved by examining the normalised difference in the peak powers off all trials and performing a one-sample t-test on these differences, with a null-hypothesis that the mean of the differences is 0 and a significance value of 0.05. The normalised difference is obtained by dividing the difference between P_{Sim} and P_{Meas} of a stroke by the respective P_{Meas}. We also displayed these power differences in a boxplot to see the median error of the 7-steps kinematic-only methodology.

4 Results

4.1 Scaling and Inverse Kinematics

The scaled model of each participant is presented in Figure 4.1. Note that the PAS marker was placed 4-5cm forward (x direction) in the model with respect to the measured marker in the static pose. This was done as the marker would otherwise end up inside the knee (not possible). As the OpenSim model bodies were scaled according to the OpenSim guidelines, and the positioning of the legs is largely determined by the other leg markers, this repositioning of the PAS marker was acceptable.

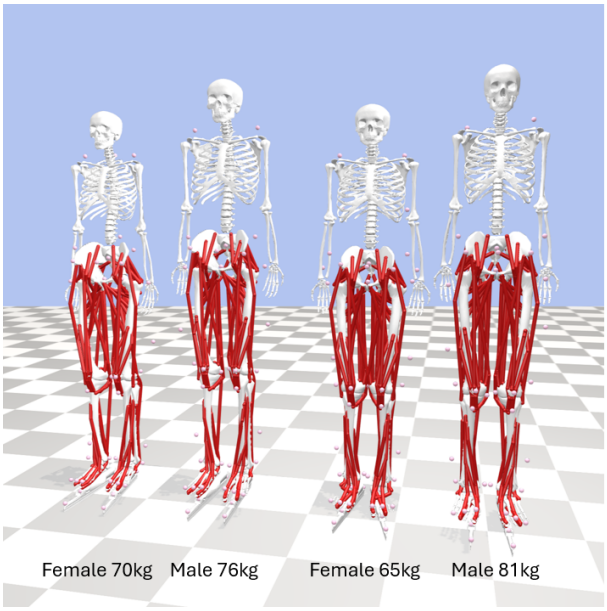

Figure 4.1: Scaled OpenSim Rajagopal [18] and skate model.

After running the Inverse Kinematics Tool in OpenSim with a marker weight of 1 we found that the mean marker error, the difference between model markers and experimental markers, for all the experiments was between 2.5-3.5 centimeters, with the maximum error typically occurring between 5 and 10 centimeters (Figure 4.2). Furthermore, the error in the center of mass of the body and the skates was between 2.5-3.5 centimeters (Figure 4.3).

These large errors ($\approx$ 10cm) were instantaneously found in the SACR data recording, which indicated an erratic recording, in which case the sacrum marker was excluded in the following inverse kinematics iterations. Furthermore, a large marker error (($\approx$ 10cm) was found for the PAS marker and the SAE-, C7- THIGH- and AnkleIMU markers, as expected.

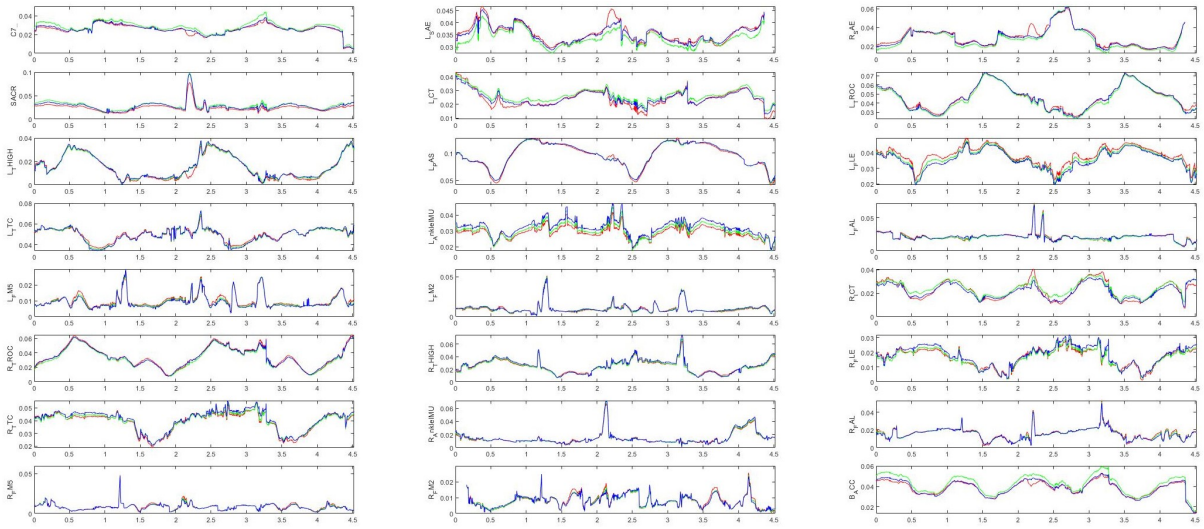

Figure 4.2: Difference between model- and experimental markers (i.e. Marker Error) [meter] over the duration of the trial [sec] Female 70kg Lap Medium 1. Blue line: All Markers = 1. Red line: SAE and C7 = 0.8, thigh and ankle IMU = 0.9. Green line: SAE and C7 = 0.5, thigh and ankle IMU = 0.7.

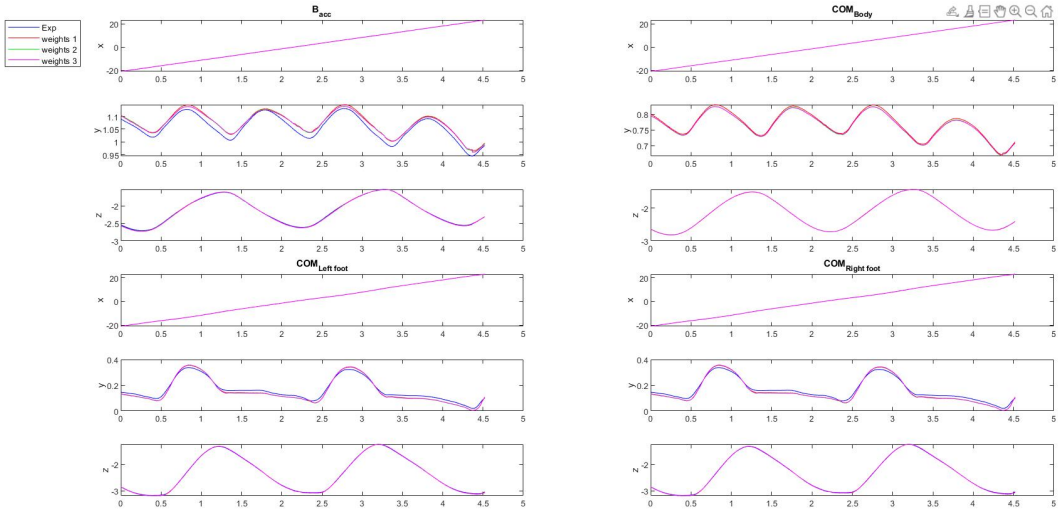

Figure 4.3: COM positions [meter] for different weight values in the Inverse Kinematics Tool over the duration of the trial [sec]. Red line: SAE and C7 = 0.8, thigh and ankle IMU = 0.9. Green line: SAE and C7 = 0.5, thigh and ankle IMU = 0.7. Pink line: SAE and C7 = 0.7, thigh and ankle IMU = 0.5.

Reducing the weights from 1 to values between 0.9 and 0.5 (as shown in Figure 4.3) did not result in a notable reduction in the marker error. Moreover, it was observed that a reduction in marker weights had a relatively minor impact on the center of mass, as shown in Figure 4.3 and thus on the simple skater model force output. Therefore, we conclude that we can run all the Inverse Kinematic trials with marker weights of 1.

This is the first occasion on which data from skaters has been incorporated into OpenSim. A representative snapshot of the stroke for one of the trials is provided in Figure 4.4.

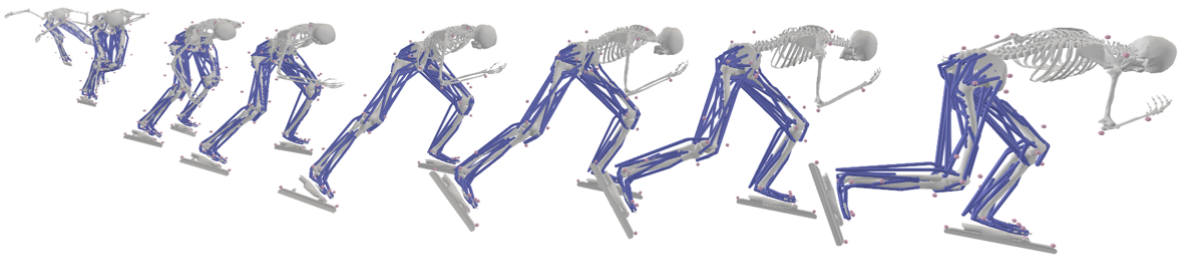

Figure 4.4: Snapshots of the stroke of the Female 65kg participant in trial Lap 1. It is noteworthy that this participant was the only subject among the four to incorporate arm movement, which was guided by a marker placed on the elbow and wrist.

4.2 Forces

4.2.1 Simple Skater Model Optimization

The mechanical constants that followed from our optimization steps are shown in Table 4.1. The model only fitted the forces to a completed stroke. Therefore, in many instances, the first and last (partially recorded) stroke in a trial is not included.

Female 70kg	Med 1	Slow 1	Slow 2	Slow 3					
Lap	2 to 5	2 to 5	2 to 5	2 to 5					
Mass Distr Coeff	0.37	0.44	0.29	0.21					
Friction Coeff	0.51	0.46	0.21	0.21					
Jmin [*10^-3]	0.14	0.15	0.17	0.21					
JminForce	0.05	0.06	0.07	0.08					
Female 65kg	Lap 1	Lap 2	Lap 4	Lap 6	Lap 7	Med 1	Med 2	Med 3	Med 4
Lap	2 to 5	2 to 4	2 to 6	2 to 5	2 to 5	2 to 5	2 to 4	2 to 4	2 to 4
Mass Distr Coeff	0.30	0.11	0.76	0.78	0.39	0.62	0.44	0.64	0.26
Friction Coeff	0.10	0.10	0.91	0.46	0.24	0.27	0.13	0.16	0.10
Jmin [*10^-3]	0.10	0.10	0.18	0.16	0.31	0.11	0.12	0.16	0.26
JminForce	0.04	0.04	0.07	0.06	0.11	0.04	0.04	0.05	0.07
Male 76kg	Lap 1	Lap 2	Lap 5	Fast 1	Fast 2	Fast 3	Med 1	Med 2	Med 3
Lap	2 to 5	3 to 7	2 to 4	3 to 4	2 to 3	2 to 4	2 to 5	2 to 3	3 to 5
Mass Distr Coeff	0.42	0.11	0.51	0.38	0.43	0.40	0.36	0.07	0.39
Friction Coeff	0.10	0.10	0.35	0.16	0.19	0.25	0.38	0.12	0.38
Jmin [*10^-3]	0.06	0.12	0.07	0.04	0.06	0.07	0.09	0.19	0.10
JminForce	0.03	0.04	0.02	0.01	0.01	0.02	0.03	0.04	0.03
Male 81kg	Lap 1	Fast 1	Fast 2	Fast 3	Fast 4	Slow 1	Slow 2	Slow 3	
Lap	1 to 2	2 to 4	2 to 4	2 to 4	2 to 3	2 to 3	2 to 3	2 to 3	
Mass Distr Coeff	0.15	0.57	0.12	0.50	0.48	0.50	0.15	0.54	
Friction Coeff	0.10	0.39	0.10	0.15	0.10	0.11	0.12	0.10	
Jmin [*10^-3]	0.21	0.30	0.20	0.13	0.13	0.10	0.18	0.07	
JminForce	0.05	0.08	0.7	0.05	0.03	0.03	0.05	0.02	

Table 4.1: Coefficients, Jmin errors and force errors

4.2.2 Mass distribution and air friction coefficient variations

However, we noticed that the mass distribution coefficient values for the simple skater model found through optimisation for Jmin is in some trials higher (Table 4.1) than we would expect. Furthermore, we found a large range for the mass distribution coefficient between the trials of one participant (e.g. female 65kg: mass distribution coefficient between 0.11-0.78), whereas this coefficient should be more or less the same. To explore this range, we plotted the forces (shown in Figure 4.5,Figure 4.6) and the total joint power (shown in Figure 4.7, Figure 4.8) for a variety of coefficients.

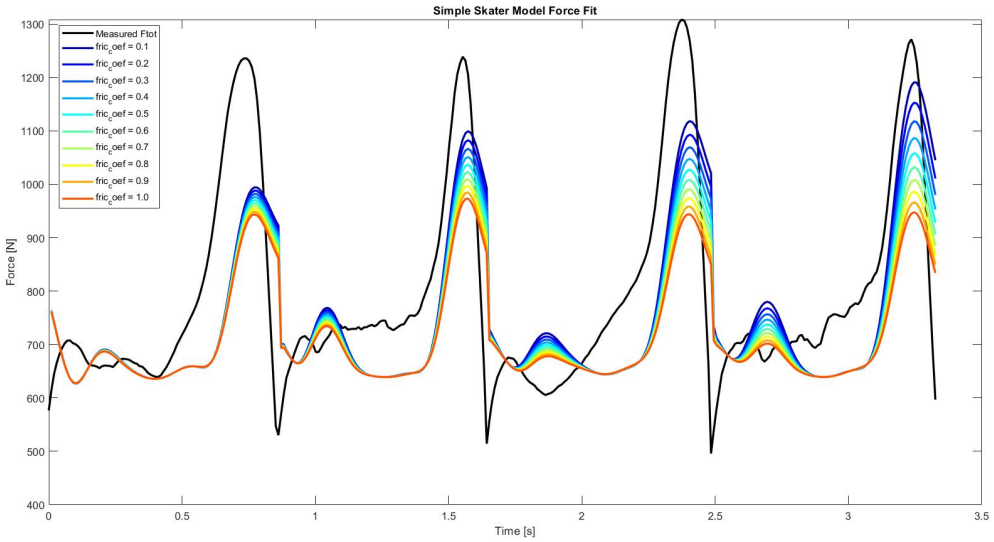

Figure 4.5: Forces given by the Simple Skater Model for the 65kg Female in Lap 4: The black line represents the measured forces, the colored lines represent a friction coefficient value from 0.1-1

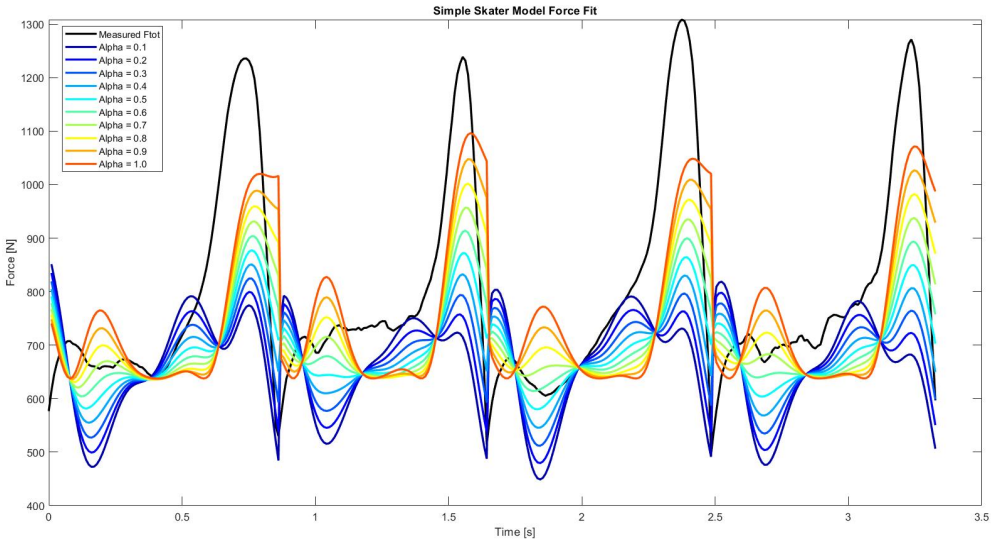

Figure 4.6: Forces given by the Simple Skater Model for the 65kg Female in Lap 4: The black line represents the measured forces, the colored lines represent a mass distribution value alpha from 0.1-1

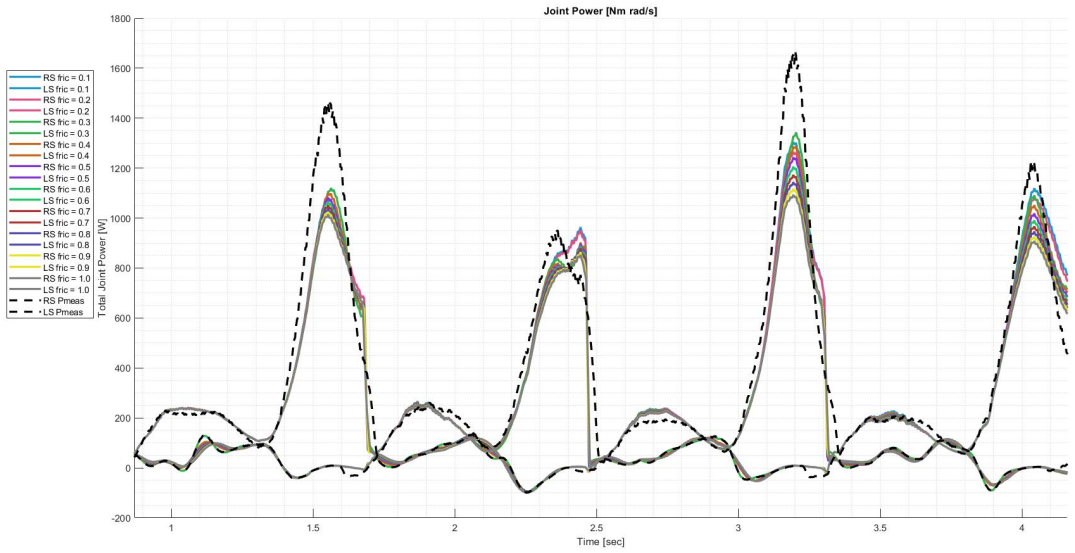

Figure 4.7: Power given by the Simple Skater Model for the 65kg Female in Lap 4: The black dotted line represents the measured forces, the colored lines represent a friction coefficient value from 0.1-1

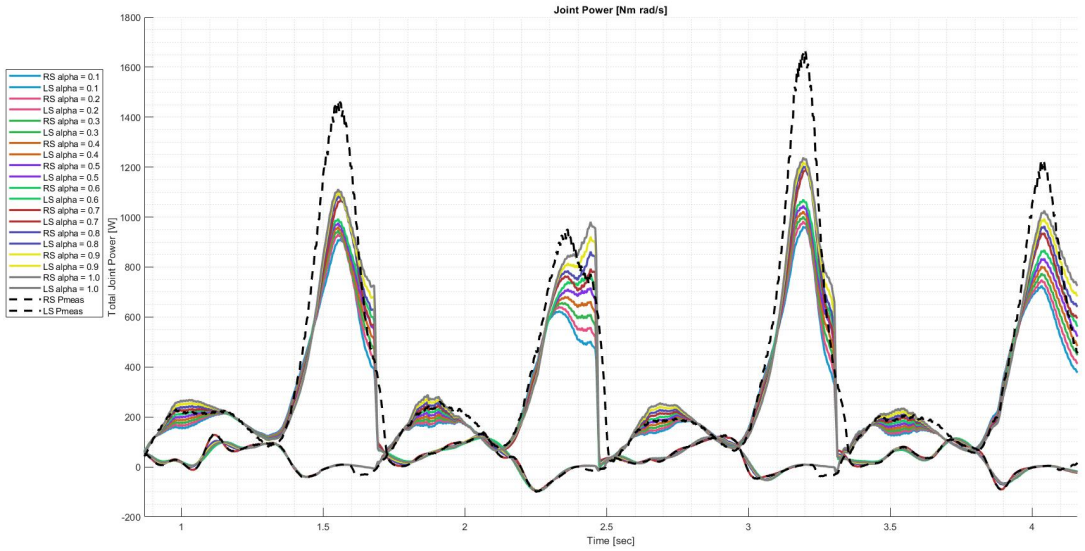

Figure 4.8: Power given by the Simple Skater Model for the 65kg Female in Lap 4: The black line dotted represents the measured forces, the colored lines represent a mass distribution value alpha from 0.1-1

4.2.3 Difference between Measured and Modelled forces

In table 4.1 the Root Mean Square Error between the measured and modelled (Simple Skater Model) resultant force trajectories over all the trials per participant are displayed.

RMSE [N]	Force		No. Strokes	
Participant	Left	Right	Left	Right
70kg female	131.5	141.7	7	8
65kg female	124.3	120.6	16	13
76kg male	117.0	100.5	12	13
81kg male	154.9	124.1	11	7

Table 4.2: Root Mean Square Error (RMSE) between the measured and modeled resultant force trajectories over all trials per participant, divided over left and right strokes. No.Strokes: Number of strokes the RMSE was based on

4.3 Inverse Dynamics

4.3.1 Difference between Mean and Measured Center of Pressure

The mean CoP of all the right skate strokes (mm) of the 70kg Female participant, normalised to stroke length(%), with 0mm located on the $Blade_End$ marker is shown in Figure 4.9 by the black line and in Figure 4.10 by the red dotted line. Furthermore, Figure 4.10 shows the mean CoP of all the right skate strokes of all the four participants combined (solid red line), the left skate strokes(solid blue line) and both left and right strokes combined (black lines).

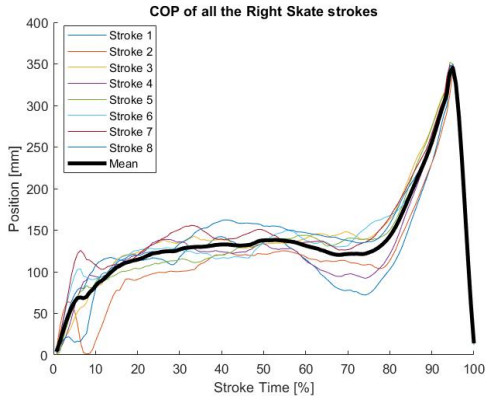

Figure 4.9: Mean Center of Pressure of all the right skate strokes of the 70kg Female normalised to stroke length (%)

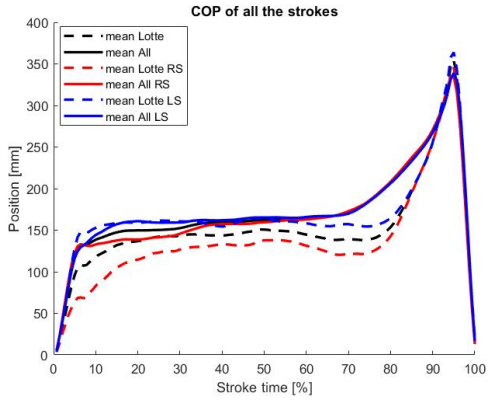

Figure 4.10: Mean Center of Pressure of all the strokes of all participants normalised to stroke length (%)

With these mean CoP values and the modeled push-off forces we calculated the power with the kinematic-only methodology, as illustrated in Figure 4.11.

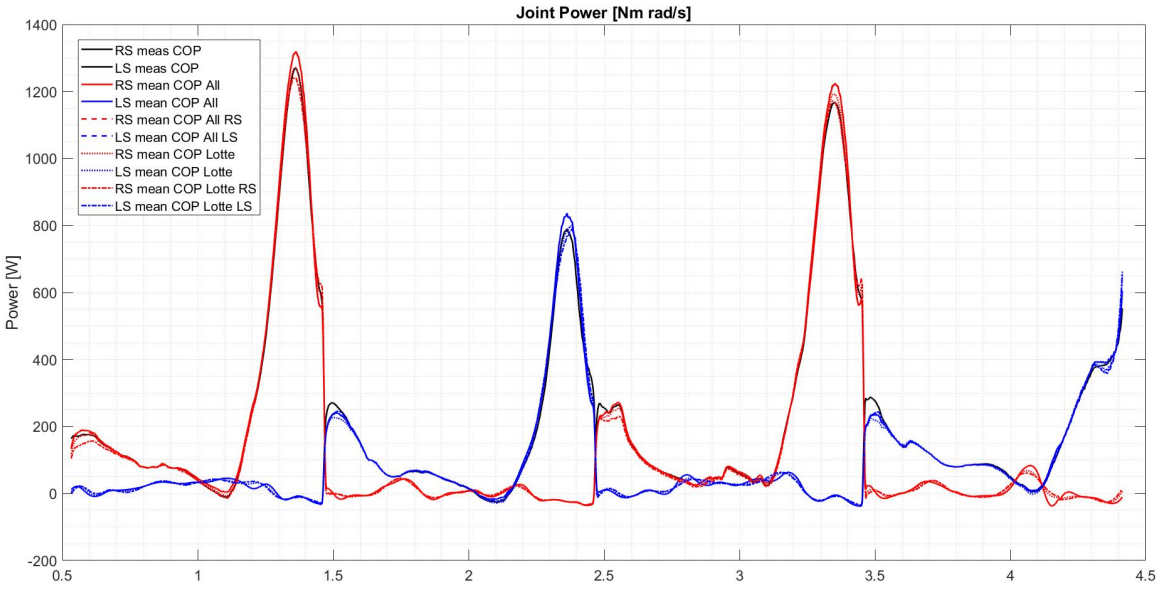

Figure 4.11: Mechanical power calculated with modeled push-off forces, using the measured CoP or the mean CoP as inputs.

4.3.2 Power Assesment

The measured push-off forces, calculated joint powers of all the joints (hip, knee, ankle) and the sum of these joint powers (total joint power) of one trial is illustrated in Figure 4.12. We noticed that the power error, the difference between P_{Sim} and P_{Meas}, is a sum of power errors on every joint. Nevertheless, the largest contribution to this power error seems ($\approx$ 25-30%) to be the hip flexion power Figure A.19. In all the trials (plotted in section A.3), the patterns of these joint powers are similar to those found in the literature by visual inspection[5][6].

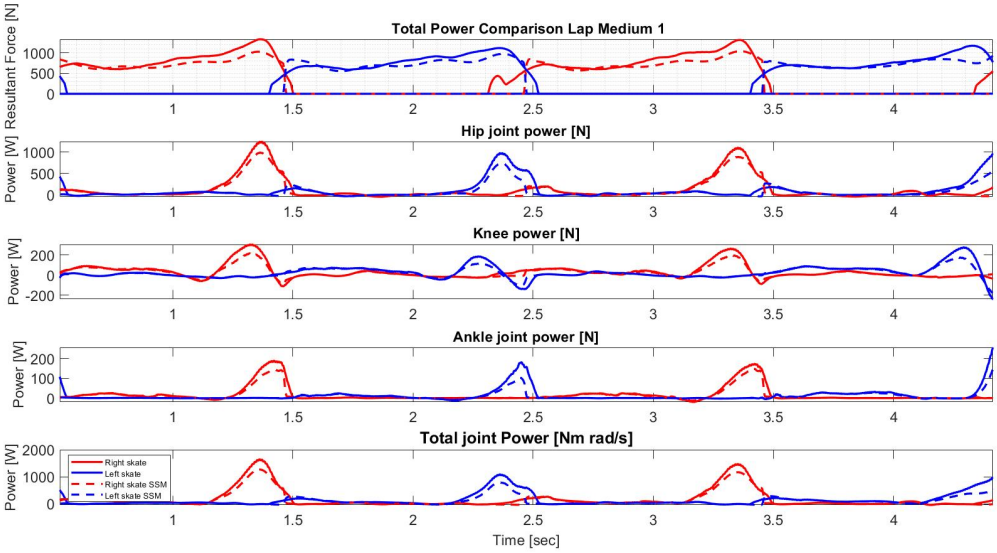

Figure 4.12: 3D Joint Power using measured forces of a 70kg Female during trial: Lap Medium 1

4.4 Statistics

In Figure 4.12, we note that the main difference in total power occurs at the end of the stroke. The normalised difference between peak P_{Sim} and peak P_{Meas} is shown in Figure 4.13, together with the p-value from the One-Sample t-test. It is shown that the interquartile range (IQR) of the errors for all strokes of all participants combined (5th box) is between 10.7% and 24.5% with a median of 18.8% . Furthermore, we note that the p-values are smaller than the significance value of 0.05.

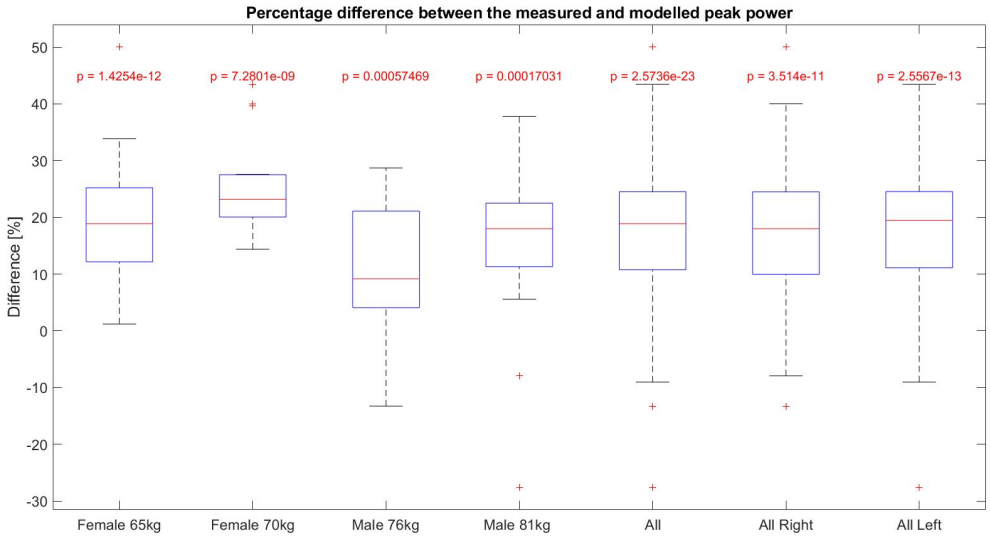

Figure 4.13: Boxplot representation of the difference between the peak mechanical power calculated using the simple skater model forces and the mechanical power calculated using the actual measured forces of all trials, categorized by participant. We notice that all the p-values are smaller than the significance level of 0.05, therefore there is a significant difference in peak power between P_{Sim} and peak P_{Meas}

5 Discussion

This research aimed to develop a Matlab-based pipeline for assessing mechanical power in long-track speed skating based on solely kinematic data as input. We proposed a 7-step pipeline, based on an inverse analysis with the use of a musculoskeletal model, the force input from the validated Simple Skater Model [1], and the joint angles and center of masses of the participant's body and skates from a kinematic recording.

Our method was validated by using this 7-step approach to calculate the mechanical power with the forces from the simple skater model and with the measured forces [1] and comparing the difference between the peaks of these two powers for all the trials using a statistic One-Sample t-test.

According to the statistical tests (section 4.4), there is a significant difference between the simulated-(P_{sim}) and measured- (P_{meas}) peak power ($p<0.05$). Furthermore, we noticed a positive interquartile range (IQR) of these error percentages between 10.7% and 24.5% for all participants combined. This is quite a wide range.

We did see that for 3 of the 4 participants, the median error was quite consistent (18.9%, 23.1%, and 18.0%). A step in future research would be to add the median error (18.9%) to the modeled power to correct the results.

Nevertheless, a consistent error margin is an acceptable compromise. The objective is to utilize the mechanical power in combination with the forward velocity of the skater to ascertain the efficiency of the technique and observe its evolution over time in a training/competition environment when modifications are made to the training schedule and technique. The primary interest is in obtaining a readily quantifiable estimate of the power.

5.0.1 Scaling and Inverse Kinematics

This paper presented the first incorporation of data from skaters into OpenSim. The inverse kinematics tool resulted in a motion with quite large marker errors (max 5-7cm) that could not be remedied by reducing the marker weights. This might influence the representation of the correct joint angles over time, i.e. the angular joint velocities, needed in the power calculation. However, in this paper, we focused on validating our pipeline, and thus the same joint angle velocities were used for the P_{sim} and P_{meas} calculation.

Furthermore, the impact of this marker error on the determination of the center of mass of the body and skates was investigated. It was observed that a reduction in marker weights had a relatively minor impact on the center of masses, and thus on the simple

skater model force output.

5.0.2 Forces

We noticed that the coefficient values for the simple skater model found through optimization for Jmin are in some trials higher (Table 4.1) than we would expect (mass distr>0.6, fric coef>0.3). Furthermore, we found a large range for the coefficients between the trials of one participant (e.g. female 65kg: mass distribution coefficient between 0.11-0.78). Upon examination of the impact of these coefficient variations on the modeled force (Figure 4.5.Figure 4.6), it becomes evident that in the trials with a high coefficient, the measured force is significantly higher than the modeled value, rendering a match impossible. The reason for this remains unclear for now.

In the future, we should focus on using one value for the mass distribution coefficient per participant, perhaps derived from the individuals' body proportions. Furthermore, we should try to derive the friction coefficient from the frontal area of the skater, which can be observed with the kinematic measuring equipment, and the drag coefficient for a given skating position Cd [16].

5.0.3 Inverse Dynamics

There is a lot of inconsistency and imprecision found in the determination of joint power, resulting from inverse dynamics methods, incorporation of translational joint powers, partitioning in negative and positive work, and power flow between segments [19]. In our pipeline, we chose to calculate the mechanical power (from joint angular velocity and joint moment) produced by the lower limb (hip, knee, ankle) with an OpenSim Rajagopal [18], only considering the rotational degrees of freedom (hip:3, knee:1, ankle:2). As we are in the process of validating our pipeline, it is sufficient to employ the same method for both the P_{sim} and P_{meas}.

From a visual inspection, it seemed that a large part of the power error ($\approx$ 25-30%) was due to the hip flexion power. A future step would be to perform a One-Sample t-test on the differences in P_{sim} and P_{meas} on a joint level (ankle, knee, hip) to confirm this statement.

Furthermore, we have shown that using the mean center of pressure location instead of the measured location does not influence the power by a significant amount. Therefore, it is likely that future implementations of this proposed pipeline can use a predefined mean CoP equation.

5.0.4 Power assessment

It was observed that often the power produced by the right leg is greater than the power produced by the left leg, as shown in section A.2. It can be observed that the RMSE of forces do not differ in the same manner (section 4.2); however, a small difference in angular joint velocity between left and right is evident Figure A.21. This is an interesting

observation that should be investigated further. The discrepancy may be attributed to the leg dominance of the specific skater or to the fact that the skaters turn left each corner, resulting in one leg being stronger than the other.

5.0.5 Muscle Power and Activation

The analysis of individual muscle forces and activations during the stroke provides invaluable insights to athletes and coaches, which can be applied to enhance technique, adapt training programs, and develop additional speed skating-specific training movements outside the ice rink. Consequently, the future steps for this research will be to utilize the "static optimization tool" from OpenSim and subsequently analyze the resulting data. However. currently, there is no model or data available representing the muscle parameters and mass distribution of athletes, let alone a skater [12]. Furthermore, the available open-source models represent males, not females [12]. Therefore, the muscle activations and muscle powers calculated with this model might not be the best representation of the skaters. A first attempt at running the static optimization tool failed with the message "The model appears too weak for static optimization".

6 | Conclusion

In this research we showed:

- The introduction of a ready-made Matlab-based pipeline for assessing mechanical power in long-track speed skating based on solely kinematic data as input.
- The development of a musculoskeletal OpenSim model representing a skater, to be used in our pipeline, by combining a self-made klapskate model to an opensource musculoskeletal model [18].
- The incorporation of data from skaters into OpenSim for the first time
- The presentation of a comparitive analysis of the joint power following from our pipeline with a kinematic-only based input and a measured input.
- The results of the comparitive analysis, indicating a significant difference ($p<0.05$) with the kinematic-only method underestimating the mechanical power between 10.7% and 24.5% for all participants, and for 3 of the 4 participants, a quite consistent median error of 18.9%, 23.1%, and 18.0%.
- An observation that the power produced by the right leg is greater than the power produced by the left leg, to be looked into further.

The implementation of this proposed timeline is to utilize the mechanical power in combination with the forward velocity of the skater to ascertain the efficiency of the technique and observe its evolution over time in a training/competition environment when modifications are made to the training schedule and technique. The primary interest of obtaining a readily quantifiable estimate of the power was met, which brought us one step closer to a video-to-power implementation. Future steps for this research are:

- Investigate what the main contributor is for the peak power error on a joint level by performing a One-Sample t-test on the power components (hip adduction power, knee flexion power etcetera)
- Continue to investigate the reason why the peak power of the right leg is greater than that of the left leg.
- Investigate individual muscle forces and activations utilizing the static optimisation tool in Opensim, although this may not provide the most accurate representation due to the inherent limitations of the musculoskeletal model.

.

References

[1] E. van der Kruk, H. E. J. Veeger, F. C. T. van der Helm, and A. L. Schwab. Design and verification of a simple 3D dynamic model of speed skating which mimics observed forces and motions. *J. Biomech.*, 64:93–102, November 2017.

[2] V.G. de Vette, D. Veeger, and M.P. van Dijk. Using wearable sensors to estimate mechanical power output in cyclical sports other than cycling—a review. *Sensors*, 23(1), 2023.

[3] Sebastian Sitko, Rafel Cirer-Sastre, Francisco Corbi, and Isaac López-Laval. Power Assessment in Road Cycling: A Narrative Review. *Sustainability*, 12(12):5216, June 2020.

[4] J. J. de Koning, G. de Groot, and G. J. van Ingen Schenau. Coordination of leg muscles during speed skating. *J. Biomech.*, 24(2):137–146, 1991.

[5] H. Houdijk, J. J. de Koning, G. de Groot, M. F. Bobbert, , , and G. J. van Ingen Schenau. Push-off mechanics in speed skating with conventional skates and klapskates. *Med. Sci. Sports Exerc.*, 32(3):635–641, March 2000.

[6] R. W. de Boer, J. Cabri, W. Vaes, J. P. Clarijs, A. P. Hollander, G. de Groot, and G. J. van Ingen Schenau. Moments of force, power, and muscle coordination in speed-skating. *Int. J. Sports Med.*, 8(6):371–378, December 1987.

[7] Marian Bittner, Wei-Tse Yang, Xucong Zhang, Ajay Seth, Jan Van Gemert, and Frans C. T. Van Der Helm. Towards single camera human 3d-kinematics. *Sensors*, 23(1):341, December 2022.

[8] Zhi-Yi Lin, Bofan Lyu, Judith Cueto Fernandez, Eline van der Kruk, Ajay Seth, and Xucong Zhang. 3D Kinematics Estimation from Video with a Biomechanical Model and Synthetic Training Data. In *2024 IEEE/CVF Conference on Computer Vision and Pattern Recognition* , pages 1441–1450. IEEE, June 2024.

[9] The MathWorks Inc. Matlab version: 9.13.0 (r2022b), 2022.

[10] Scott L. Delp, Frank C. Anderson, Allison S. Arnold, Peter Loan, Ayman Habib, Chand T. John, Eran Guendelman, and Darryl G. Thelen. OpenSim: open-source software to create and analyze dynamic simulations of movement. *IEEE Trans. Biomed. Eng.*, 54(11):1940–1950, November 2007.

[11] Musculoskeletal Models - OpenSim Documentation - OpenSim, October 2024. [Online; accessed 21. Oct. 2024].

[12] R. Maarleveld, H.E.J. Veeger, F.C.T. van der Helm, J. Son, R.L. Lieber, and E. van der Kruk. What the %pcsa? addressing diversity in lower-limb musculoskeletal models: Age- and sex-related differences in muscle strength parameters. *Journal of Biomechanics*, 2024. Preprint.

[13] E. van der Kruk, A. L. Schwab, F. C. T. van der Helm, and H. E. J. Veeger. Getting in shape: Reconstructing three-dimensional long-track speed skating kinematics by comparing several body pose reconstruction techniques. *J. Biomech.*, 69:103–112, March 2018.

[14] OpenSimVideos. OpenSim Webinar: Tips and Tricks for Data Collection, Scaling and Inverse Kinematics in OpenSim, April 2017. [Online; accessed 15. Sep. 2024].

[15] G. J. van Ingen Schenau. The influence of air friction in speed skating. *J. Biomech.*, 15(6):449–458, January 1982.

[16] Alexander Spoelstra, Wouter Terra, and Andrea Sciacchitano. On-site aerodynamics investigation of speed skating. *J. Wind Eng. Ind. Aerodyn.*, 239:105457, August 2023.

[17] Doris I. Miller and Richard C. Nelson. *Biomechanics of Sport: A Research Approach.* McGraw-Hill, Maidenhead, England, UK, 1973.

[18] Apoorva Rajagopal, Christopher L. Dembia, Matthew S. DeMers, Denny D. Delp, Jennifer L. Hicks, and Scott L. Delp. Full body musculoskeletal model for muscle-driven simulation of human gait. *IEEE transactions on bio-medical engineering*, 63(10):2068–2079, October 2016.

[19] E. van der Kruk, F. C. T. van der Helm, H. E. J. Veeger, and A. L. Schwab. Power in sports: A literature review on the application, assumptions, and terminology of mechanical power in sport research. *J. Biomech.*, 79:1–14, October 2018.

Appendices

A | Appendix

A.1 Static Pose Marker Weights

To position the skate under the foot, the rotation around the y-axis and displacement in the x, y, and z directions were unlocked. The rotation around the z-axis of the blade to the bridge (i.e., klapping coordinate) was locked, as the participant was standing on a closed skate. The metatarsophalangeal (MTP) angle was also locked because foot movement was constrained by the shoe. The remaining coordinates were unlocked.

High weights (100) were assigned to all added virtual markers (MFM25, AJC, KJC, HJC, MIAS, MHJC, MPELV) and the C7 marker for the static pose. The scapulae markers (SAE) were also given high weights (10), as these, together with C7, are the only markers that represent the forward flexion of the upper body.

The ankle IMU and the thigh markers, which are placed on bands rather than bony landmarks, were assigned weights of zero due to their positional freedom. The FM2 and FM5 markers were placed on the shoe, not directly on the bony landmark of the foot. Their location could only be estimated based on pictures. Therefore, they were given a weight of 0.5. The FAL and TAM marker were also placed on the shoe, but very close the the bony landmark on the ankle. Therefore these were given a weight of 0.8.

After scaling the model, the coordinates of the bridge and blade were locked again to maintain the positioning of the skate during dynamic trials, and we unlocked the "klapping coordinate."

A.2 Difference in power left and right

We categorized all the strokes based on the self-chosen low-, medium-, and high velocities as shown in Figure A.1 to Figure A.18.

We note that the stroke duration and peak power differ between strokes and that total power produced by the left and right leg is not equal. The 70kg female and 76kg male both had a more powerful right stroke. The 81kg male also showed this leg dominance on slow laps, but the left leg became more dominant on the faster laps. The 65kg female also showed a more powerful left stroke, but this was mainly caused by 1 trial higher than the other 3. In general, slower laps have a longer, less powerful stroke than faster laps. These observations are summarised in Table A.2.

Participant	Speed	Max Peak Power per Leg	Max Stroke Duration
70kg female	Fast, slow	R,R	Slow
65kg female	Med	L	
76kg male	Fast, Med	R,R	Fast
81kg male	Fast, Slow	L,R	Slow

Table A.1: Power analysis showing asymmetry between the left an right stroke power

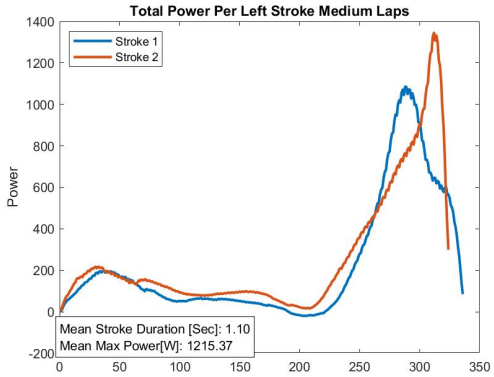

Figure A.1: Power per left stroke of a 70kg Female on the medium speed laps

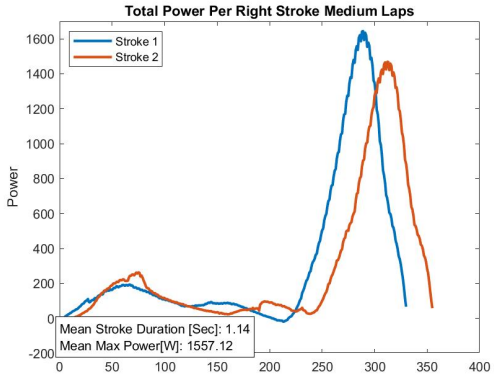

Figure A.2: Power per right stroke of a 70kg Female on the medium speed laps

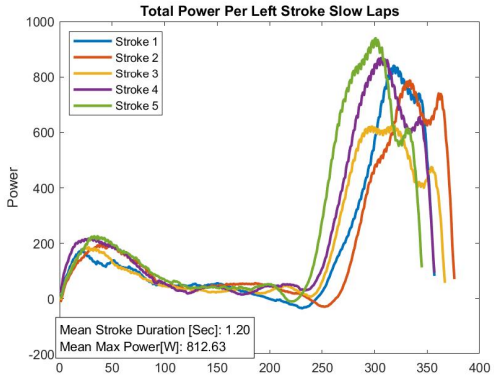

Figure A.3: Power per left stroke of a 70kg Female on the slow speed laps

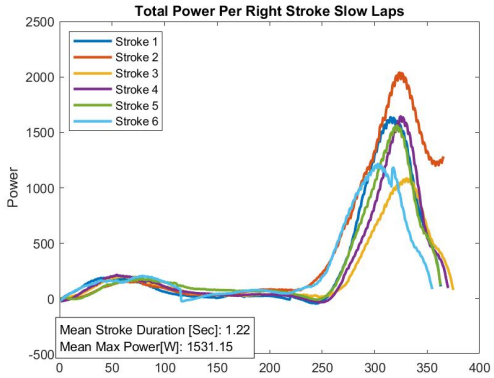

Figure A.4: Power per right stroke of a 70kg Female on the slow speed laps

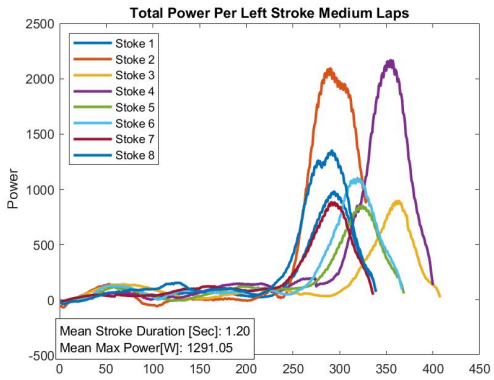

Figure A.5: Power per left stroke of a 65kg Female on the medium speed laps

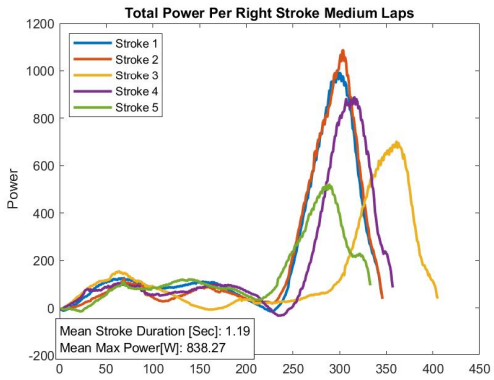

Figure A.6: Power per right stroke of a 65kg Female on the medium speed laps

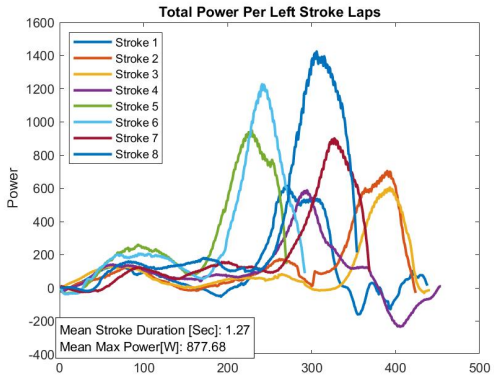

Figure A.7: Power per left stroke of a 65kg Female on the laps

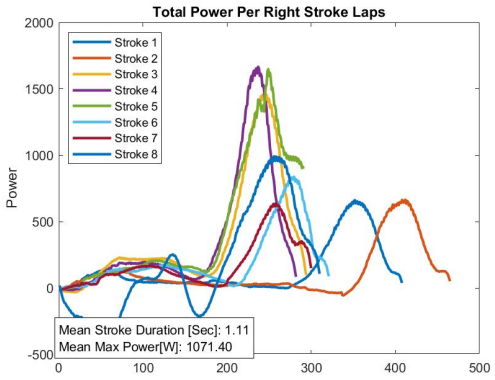

Figure A.8: Power per right stroke of a 65kg Female on the laps

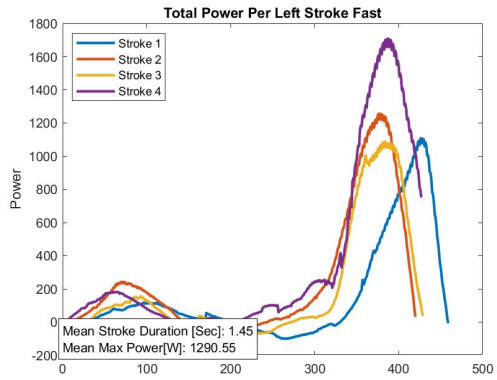

Figure A.9: Power per left stroke of a 76kg Male on the fast laps

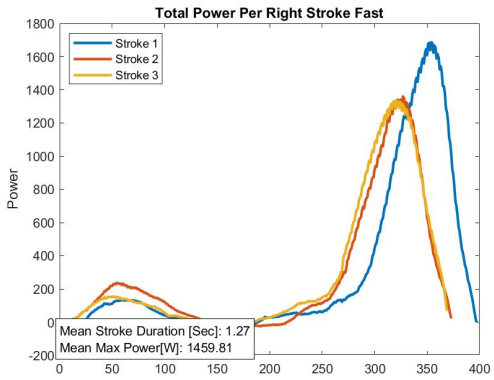

Figure A.10: Power per right stroke of a 76kg Male on the fast laps

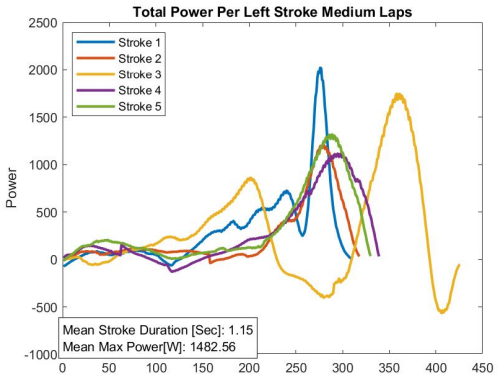

Figure A.11: Power per left stroke of a 76kg Male on the medium speed laps

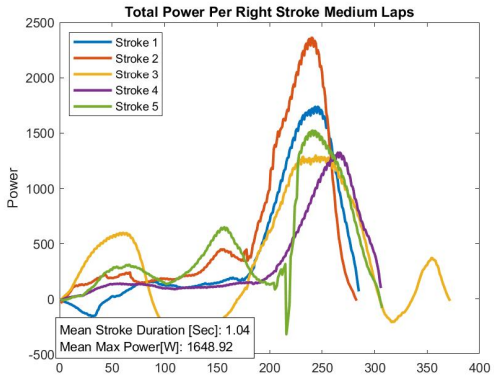

Figure A.12: Power per right stroke of a 76kg Male on the medium speed laps

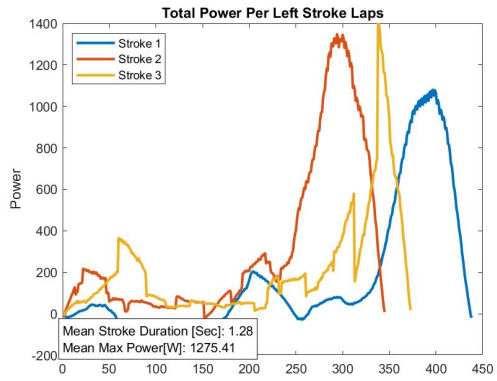

Figure A.13: Power per left stroke of a 76kg Male on the laps

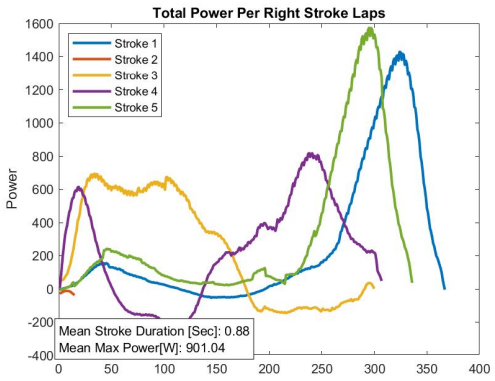

Figure A.14: Power per right stroke of a 76kg Male on the laps

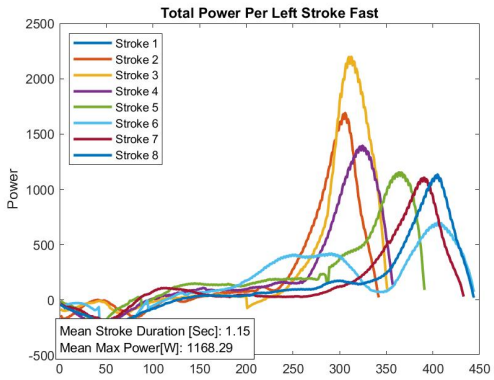

Figure A.15: Power per left stroke of a 81kg Male on the fast laps

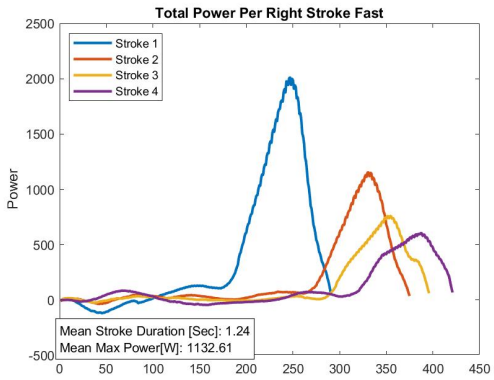

Figure A.16: Power per right stroke of a 81kg Male on the fast laps

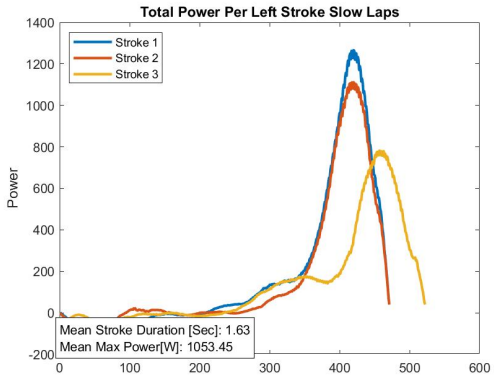

Figure A.17: Power per left stroke of a 81kg Male on the slow speed laps

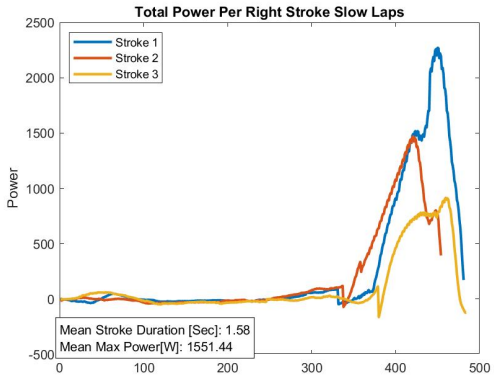

Figure A.18: Power per right stroke of a 81kg Male on the slow speed laps

A.3 Power plots measured vs SSM

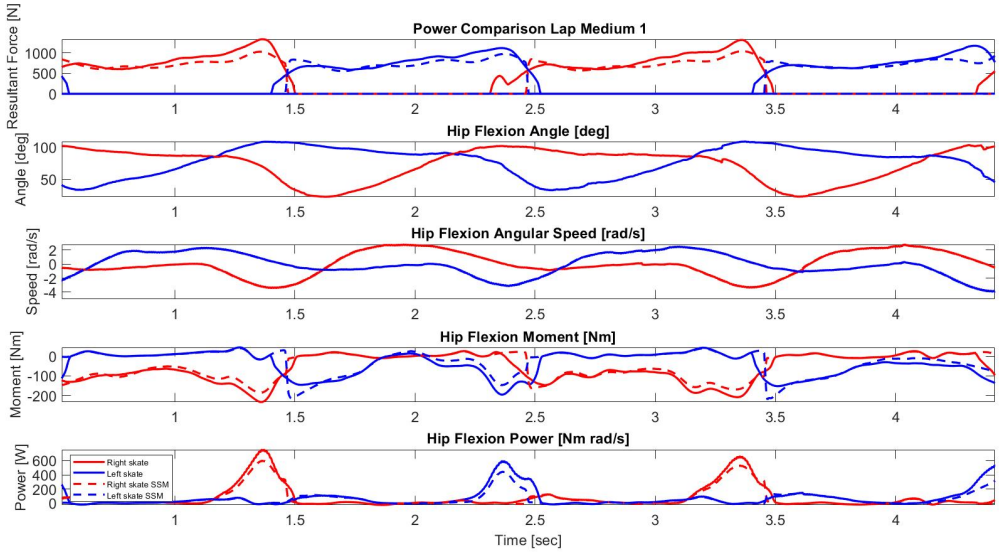

Figure A.19: Hip flexion power of a 70kg female during trial:Lap Medium 1

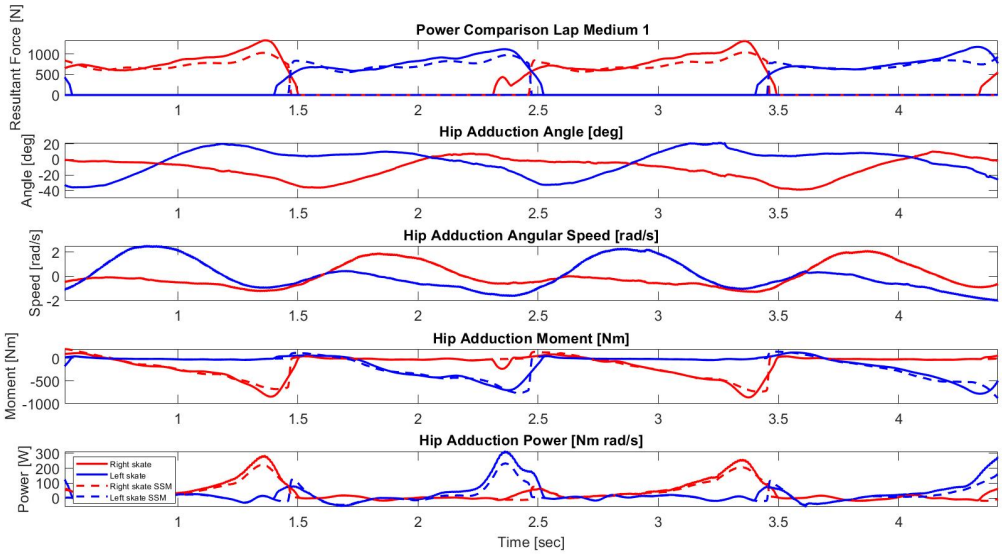

Figure A.20: Hip adduction power of a 70kg female during trial:Lap Medium 1

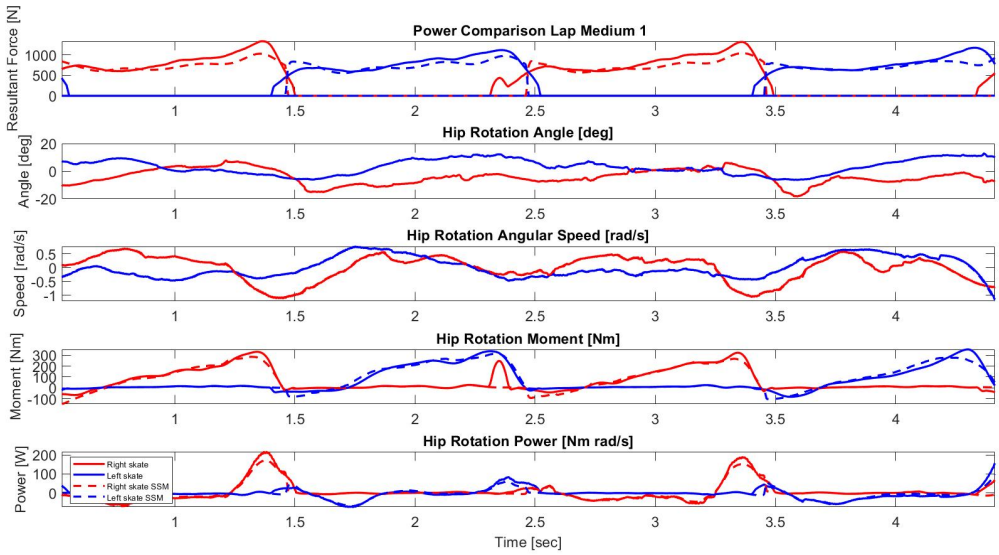

Figure A.21: Hip rotation power of a 70kg female during trial:Lap Medium 1

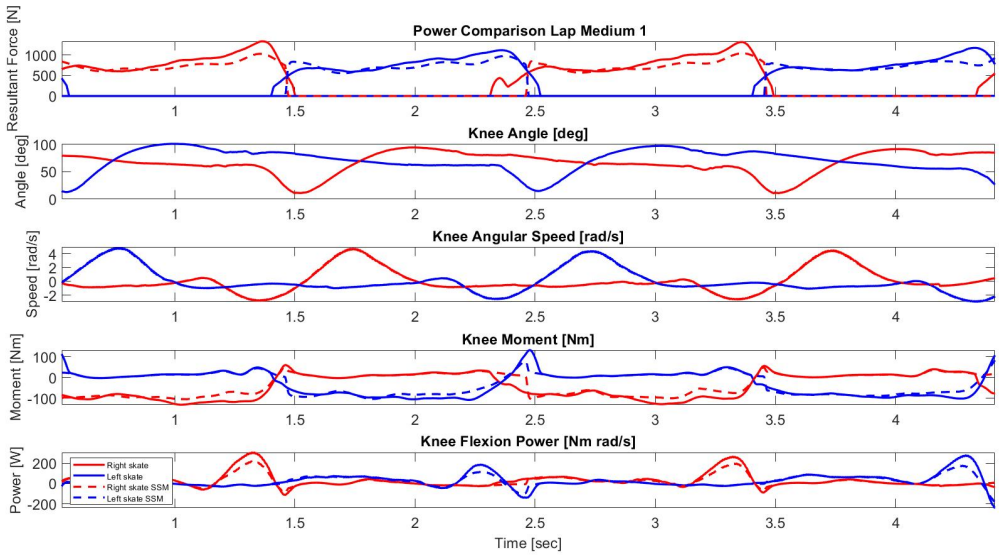

Figure A.22: Knee flexion power of a 70kg female during trial:Lap Medium 1

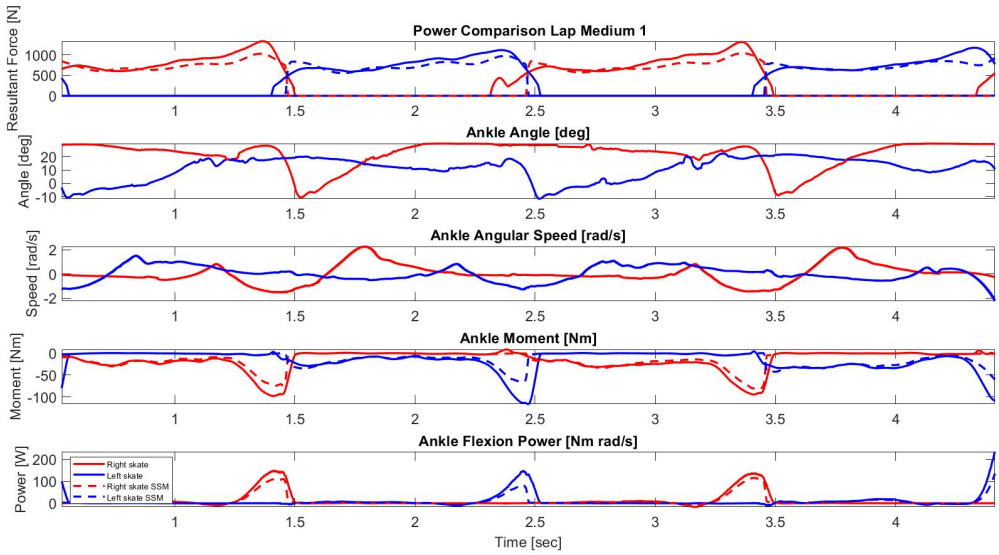

Figure A.23: Ankle flexion power of a 70kg female during trial:Lap Medium 1

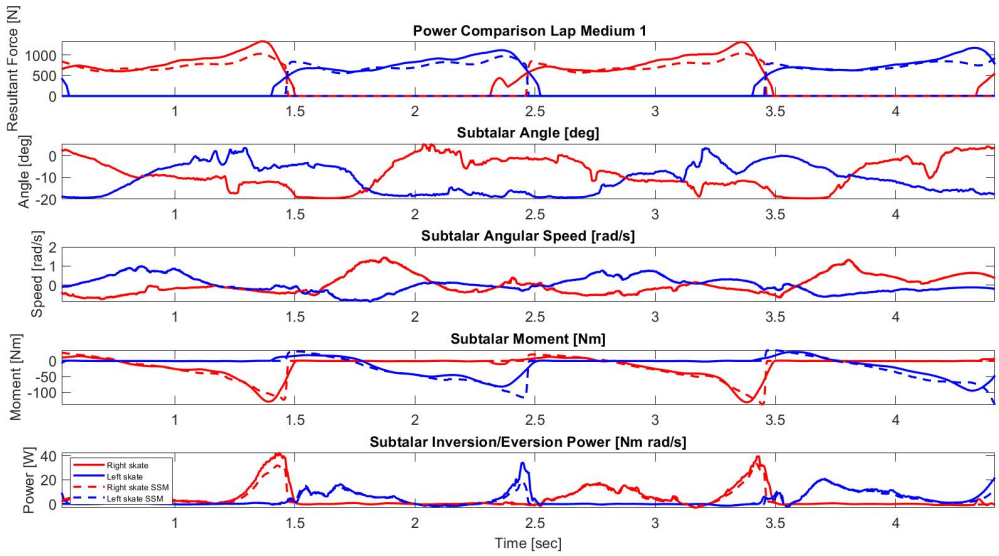

Figure A.24: Subtalar inversion/eversion power of a 70kg female during trial:Lap Medium 1

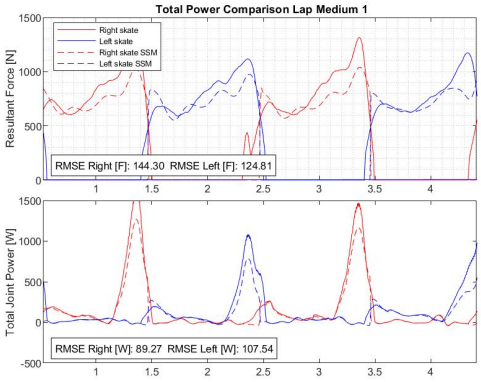

Figure A.25: Power comparison 70kg female

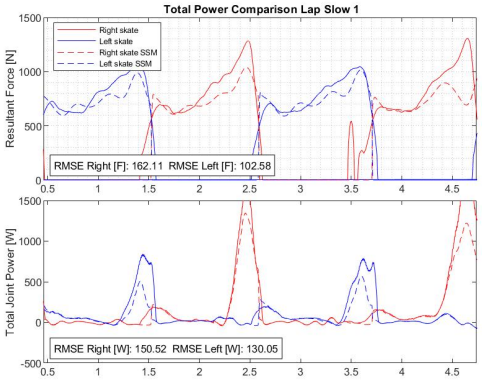

Figure A.26: Power comparison 70kg female

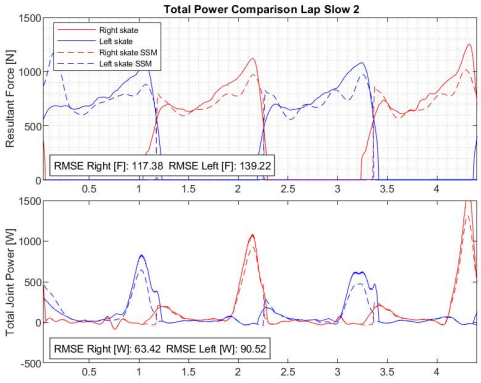

Figure A.27: Power comparison 70kg female

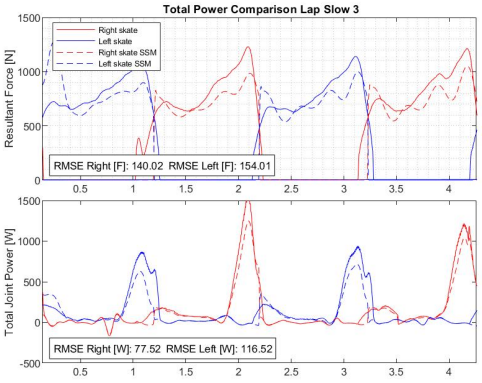

Figure A.28: Power comparison 70kg female

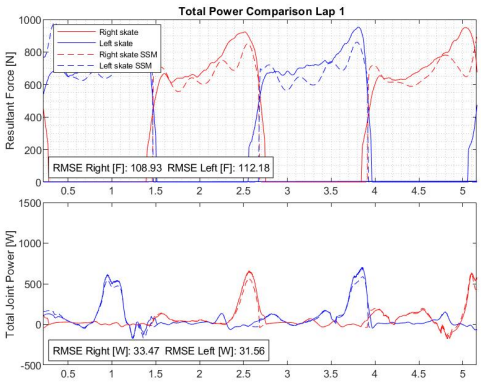

Figure A.29: Power comparison 65kg female

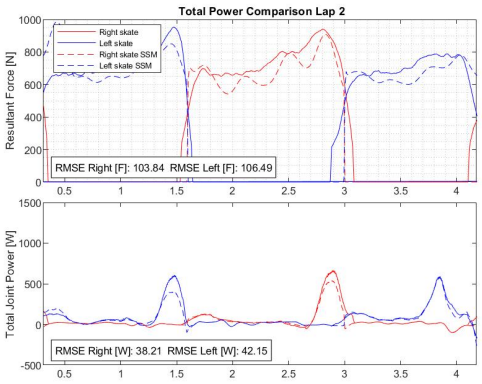

Figure A.30: Power comparison 65kg female

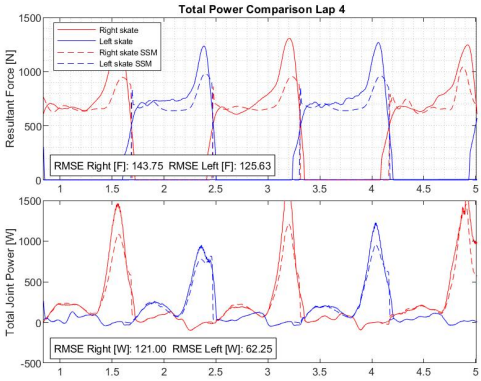

Figure A.31: Power comparison 65kg female

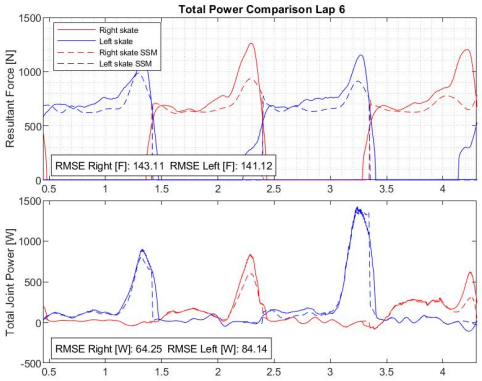

Figure A.32: Power comparison 65kg female

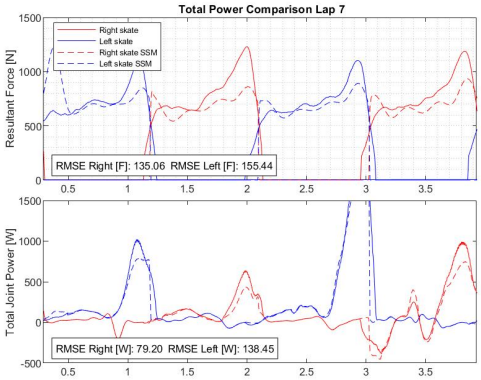

Figure A.33: Power comparison 65kg female

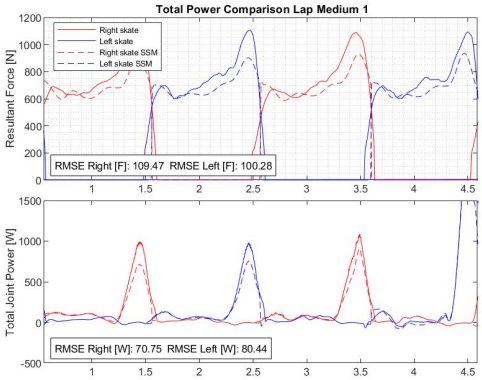

Figure A.34: Power comparison 65kg female

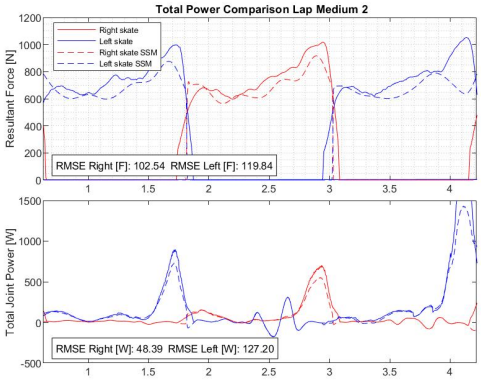

Figure A.35: Power comparison 65kg female

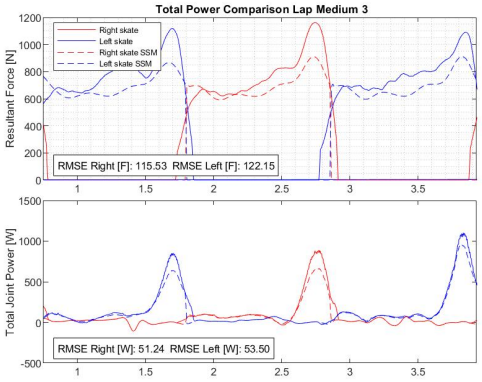

Figure A.36: Power comparison 65kg female

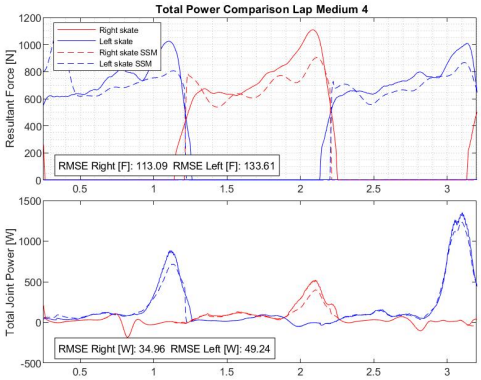

Figure A.37: Power comparison 65kg female

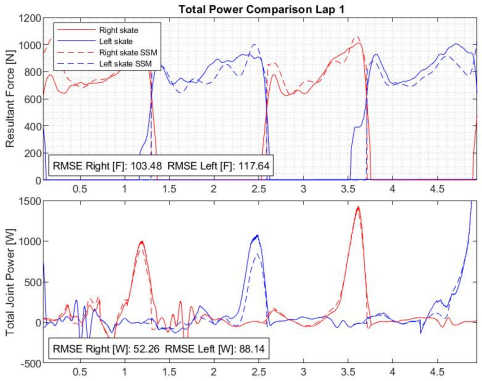

Figure A.38: Power comparison 76kg male

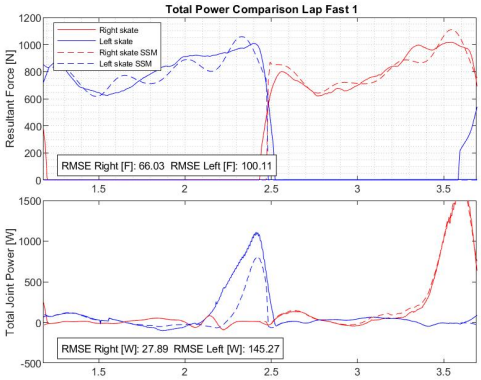

Figure A.39: Power comparison 76kg male

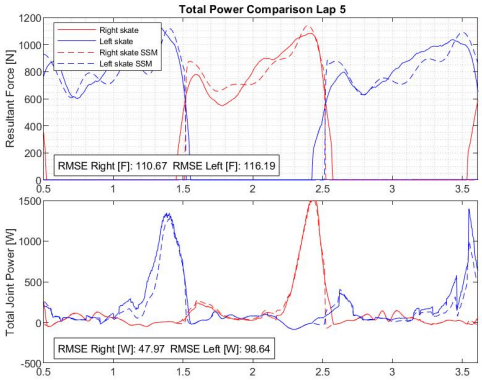

Figure A.40: Power comparison 76kg male

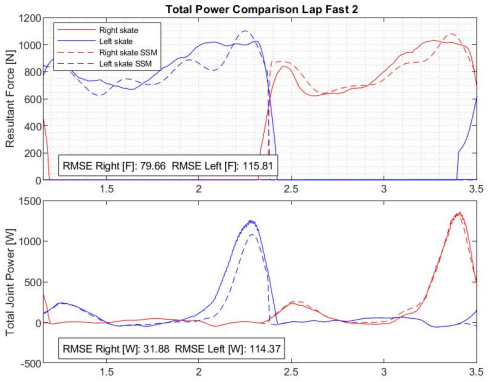

Figure A.41: Power comparison 76kg male

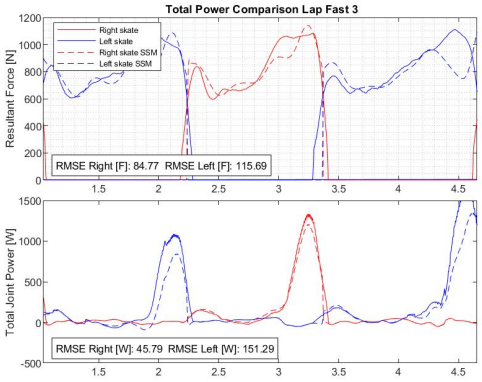

Figure A.42: Power comparison 76kg male

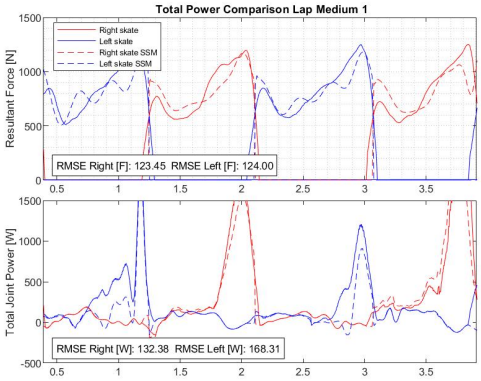

Figure A.43: Power comparison 76kg male

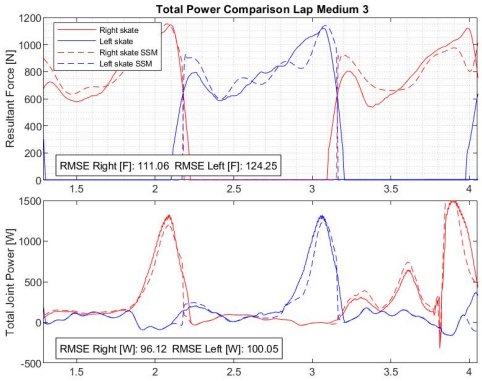

Figure A.44: Power comparison 76kg male

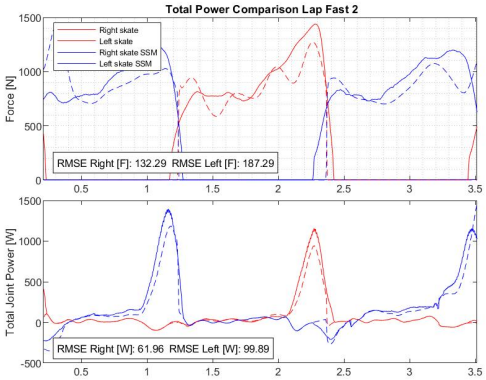

Figure A.45: Power comparison 81kg male

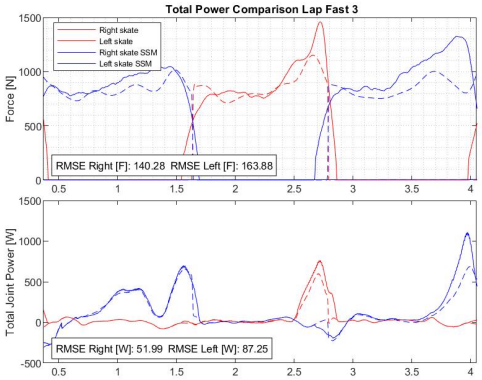

Figure A.46: Power comparison 81kg male

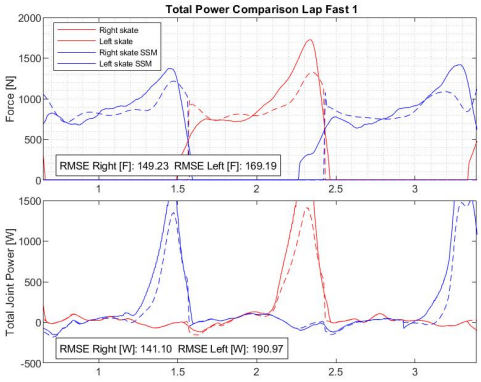

Figure A.47: Power comparison 81kg male

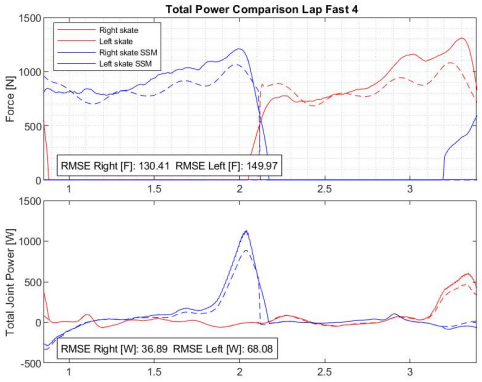

Figure A.48: Power comparison 81kg male

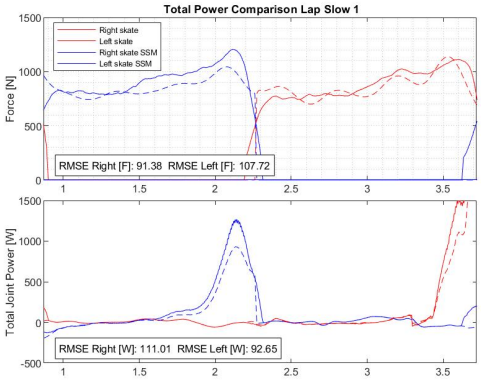

Figure A.49: Power comparison 81kg male

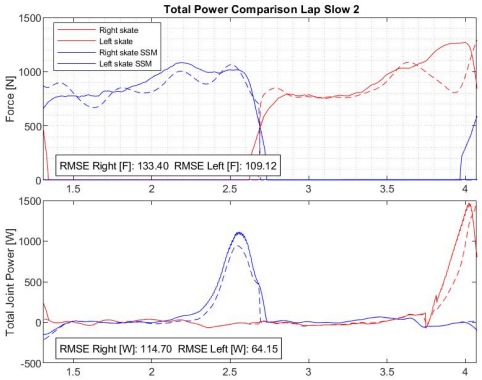

Figure A.50: Power comparison 81kg male

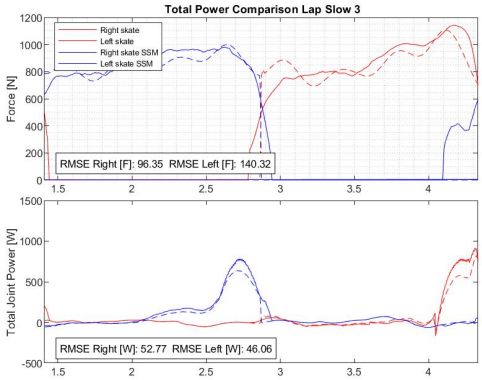

Figure A.51: Power comparison 81kg male